Simple homogenized model for the non-linear analysis of FRP strengthened masonry structures. Part I: theory

Gabriele Milani[(1)], Paulo B. Lourenço[(2)]

(1) Corresponding Author. Dipartimento di Ingegneria Strutturale (DIS), Politecnico di Milano, Piazza Leonardo da Vinci 32, 20133 Milano, Italy. E-mail: milani@stru.polimi.it
(2) ISISE, Department of Civil Engineering, School of Engineering, University of Minho, Azurém, 4800-058 Guimaraes, Portugal

Keywords: Masonry, simplified homogenization, non-linear model, SQP approach, 3D structural analysis.

Abstract

A suitable and simple two-step model able to predict the non-linear response of FRP strengthened three-dimensional masonry structures is presented. In the first step, non-strengthened masonry is substituted by a macroscopically equivalent homogeneous material through a kinematic model based on finite elements and working on a heterogeneous assemblage of blocks. Non-linearity is concentrated exclusively on joints reduced to interfaces, exhibiting a frictional behavior with limited tensile and compressive strength with softening. The homogenized stress-strain behavior evaluated at the meso-scale is then implemented at a structural level in a finite element non-linear code, relying on an assemblage of rigid infinitely resistant six-noded wedge elements and non-linear interfaces, exhibiting deterioration of the mechanical properties. FRP reinforcing strips are modeled through rigid triangles and non-linear interfaces between adjoining triangles. Delamination from the support is accounted for, by modeling FRP-masonry bond by means of non-linear softening triangular interfaces. Italian code CNR DT 200 (2004) formulas are used to evaluate peak interface tangential strength and post peak behavior. In this first part, the theoretical base of the model and the non-linear stress strain behavior at a cell level are discussed. Structural examples will be analyzed in the accompanying paper devoted to the structural scale.

1. Introduction

The foreseen inadequate performance of masonry structures under earthquakes, particularly in the case of old buildings or inadequate modern construction, is a common issue in many countries worldwide and is essentially due to the mortar joints weakness. Conventional retrofitting, such as external reinforcement with steel plates or reinforced concrete overlay, have proven to be impractical, expensive in terms of resources (time and money) and to add considerable mass to the structure (which may increase earthquake-induced inertia forces). In this context, the utilization of externally bonded FRP strips seems an interesting solution due to the limited invasiveness, durability of the FRP and good performance at failure, Korany et al. (2001), even if possible drawbacks must be also considered, namely the bond deterioration due to environmental aspects (moisture and temperature).

While FRP external reinforcement is now very popular, the prediction of its mechanical behavior when bonded to masonry in the inelastic range still remains a difficult task. Several concurring factors make the analysis of strengthened masonry structures very challenging. Among others, the most important are: (1) the heterogeneity of the masonry material, (2) the brittle behavior in tension of mortar joints, even at very low levels of external loads, (3) the delamination of the FRP from the support, which is typically brittle, and (4) the complex interaction between flexural strength and vertical pre-compression in case of bending.

At present, three different approaches may be used for the analysis of non-strengthened and FRP strengthened masonry, namely micro-models, macro-models and micro-macro (or homogenization) models.

In micro-models (Lotfi and Shing 1994, Lourenço and Rots 1997, Koutromanos et al. 2011) bricks and mortar joints are discretized separately. While micro-modeling probably reflects more precisely masonry actual behavior, the structural analyses are characterized by great computational effort and apply mostly to laboratory tests or small panels. In addition, when FRP strips are applied, the finite element (FE) discretization may become even more critical, especially with diagonal strengthening, where ad-hoc mesh refinements are required.

Macro-models (e.g. Di Pasquale 1992, Lourenço et al. 1997, Casolo 1999, Berto et al. 2002, Brasile et al. 2010) are based on the use at structural level of phenomenological constitutive laws for masonry, which is regarded as an orthotropic continuum. Despite macro-modeling is very effective from a computational point of view because large scale structural analyses may be tackled, it requires expensive laboratory characterization to effectively reflect the actual behavior of the masonry material under consideration.

Micro-macro models (Luciano and Sacco 1997, Pegon & Anthoine 1997, Colliat et al. 2002, Massart et al. 2004, Pietruszczak & Ushaksarei 2003, Milani et al. 2006a & 2006b) consider different constitutive laws for bricks and mortar joints at the meso-scale only. In this framework, a Representative Element of Volume (REV) generating the whole structure by repetition is isolated from the wall and is assumed subjected to suitable periodic and anti-periodic boundary conditions on displacement and stresses. In this way, macroscopic stress-strain relations to use at a structural level are evaluated solving a non-linear boundary value problem on a sampled REV, see Lourenço et al. (2007) for a review. Typically, a coarse FEM discretization of the REV is utilized, where displacement increments on the boundary surface are imposed, in agreement with a displacement driven procedure.

At present, it is the authors' opinion that an efficient analysis of both FRP strengthened and non-strengthened large scale masonry structures in the non-linear range requires a micro-macro or macro-computational approach (e.g. Gambarotta & Lagomarsino 1997, Pietruszczak & Ushaksarei 2002, Grande et al. 2008). Indeed, a numerical model to use at structural level should be sufficiently simple, reliable and efficient to allow the fast evaluation of (a) collapse loads, (b) displacements near collapse, (c) failure mechanism, and (d) post peak behavior of the structures.

In this paper, a simple two-step micro-macro model is used to analyze efficiently masonry FRP strengthened structures, see Figure 1. In the first step, hereafter called meso-modeling, masonry is substituted by a macroscopic equivalent material through the application of a simplified averaging procedure, in which a REV constituted by a central brick interconnected with its six neighbors through zero thickness joints is meshed with six-noded wedges and non-linear softening interfaces (mortar joints and brick-brick interfaces that allow potential internal cracks in the bricks). The approach allows to estimate in an approximate way masonry macroscopic non-linear behavior under in- and out-of-plane loads, at different orientations of the actions with respect to material axes.

In the second step, discussed in detail in Part II, full masonry structures are analyzed in the non-linear range through a tailored FE non-linear code specifically developed to conduct reliable and simple analyses on structures with any shape and under general loading conditions. Six-noded rigid and infinitely resistant wedges are utilized, e.g. Milani et al. (2009), with elastic and inelastic deformation allowed only at the interfaces between adjoining elements. Only the knowledge of masonry orthotropic stress-strain relations, i.e. information provided at the meso-scale, is therefore required.

FRP strips are modeled by means of triangular rigid elements and possible elastic and inelastic deformation is allowed only at the linear interfaces between contiguous triangles. Masonry and FRP layers interact by means of interfacial tangential actions between triangles (FRP) and wedges (masonry). There, to properly account for the detachment of the strip from the support, an elasto-damaging shear stress-slip relationship is assumed, in agreement with codes of practice formulas dealing with delamination (e.g. Italian CNR DT-200 2004).

In order to circumvent some typical drawbacks of standard FEs when dealing with softening materials, a sequential quadratic programming approach (SQP) is adopted to solve the global non-linear problem. Deteriorating masonry stress-strain curves for interfaces are approximated by means of a linear piecewise-constant discontinuous function, similarly to what proposed in Milani & Tralli (2011). At each load step, all interfaces are assumed to behave as elastic-perfectly plastic and it is therefore possible to solve the discretized non-linear problem through a standard non-linear or quadratic programming algorithm (as envisaged by, e.g., De Donato & Franchi 1973, Kaliszky

1996, Cocchetti & Maier 2003). At the end of each iteration, it is checked if some interfaces have reached a deformation (total strain) incompatible with the strength assumed for that iteration, meaning that a degradation of the ultimate stress of the interface has to be accounted. If this situation is encountered, interface strength is updated reducing its ultimate resistance to the corresponding degraded value and external loads are reduced until the corresponding QP problem reaches a feasible solution. The new starting point is represented by the displacement solution at the previous iteration. The algorithm will be tested on several medium size flat and curved FRP strengthened structures in Part II, to show the robustness of the approach in converging to the solution. Here, the theoretical basis and FEs used within the formulation are briefly recalled before the homogenized behavior –to be used at a structural level– of two masonry REVs loaded in- and out-of-plane is critically examined.

2. Numerical models for FRP-reinforced masonry: a state of the art

The analysis of entire masonry structures reinforced with external FRP strips is not an easy task and, at present, may be considered as an open issue (Luciano & Sacco 1998, Marfia & Sacco 2001). Itt can be stated that common numerical design tools are linear, limit analysis and non-linear FEM. Linear elasticity (Cecchi et al. 2004) codes are very widespread in common practice and they are nowadays considered to be a standard design tool. However, they are able to give only conventional information for masonry structures reinforced with FRP, where non-linearity occurs even at very low levels of the external loads.

The early limit analyses by Galileo and Coulomb were much diverse from the elasticity theory, in which the stress state of a structure is sought and then limited to a given threshold. As structural collapse does not usually coincide with the appearance of the first crack or the first crushing, it seems evident that linear elasticity is a regression with respect to limit analysis. Non-linear structural behavior is normally extensive and also variable with the type of structure and used materials. In addition, non-linear analysis allows estimating the collapse load of a structure and comparing it with a nominal load. A simplified form of non-linear analysis is limit analysis, which only focus on the definition of the collapse load. Examples of design methods based on limit analysis are the plastic hinge methods, the yield line method and the strut-and-tie models. Still, the widespread application of limit analysis for FRP reinforced masonry has two main obstacles: (a) formally, its application is only valid for perfectly plastic materials; (b) it gives no indication about the behavior of the structure under serviceability conditions and (c) it does not provide any information on displacements at failure. For these reasons, full non-linear analysis, which includes the successive stages, from the absence of load through the behavior under service conditions and non-linear behavior up to collapse is the most powerful form of structural analysis for static loads (Grande et al. 2008). Nonlinear mechanics and limit analysis are fields of study and research at large, which received much interest of researchers and practitioners since 1970s. The advancement of numerical techniques, mainly the Finite Element method, associated with powerful computer programs allow to satisfactorily resolve problems of increasing complexity. Currently many commercial programs contemplate nonlinear analysis (e.g. Berto et al. 2002, Massart et al. 2004, Mahini et al. 2007), which is easily accessible. However, some convergence difficulties may sometimes occur in presence of strongly non-linear problems and softening materials. In addition, its use is not straightforward since, in general, the possibilities of modern software far exceeds the knowledge available in engineers with respect to non-linear behavior of the structures. Being earthquakes a major source of damage and a recurrent extreme event, non-linear analysis is now very popular for existing structures, e.g. the seismic assessment of masonry buildings with box behavior by pushover methods (Marques & Lourenço 2011) or the seismic assessment of unreinforced masonry buildings by macro-block analysis (Lourenço et al. 2011). In addition, in many complex structures, only the numerical calculation allows to fully understand the behavior of the structure. Masonry reinforced with externally bonded FRP still requires much attention, involving its non-linear behavior brittle phenomena as delamination and joints cracking. The authors have relatively long experience in this field and recently proposed, within the homogenization theory framework, different simplified models for a numerical insight on the structural behavior of strengthened masonry, starting with studies in the linear range, passing through limit analysis (both static and kinematic) and ending with full non-linear models. As already pointed out in a general framework valid also for reinforced masonry, elastic approaches (Cecchi et al. 2004) are very simple but give little design information for this specific problem. For this reason, in an attempt to supersede the elastic approach, attention was recently focused on limit analysis (Milani et al. 2009, Milani 2009), which is able to provide some useful information at failure as for instance load multipliers and the change of the failure mechanism when FRP is introduced. Thanks to the limited numerical effort required by FE limit analysis, an interesting design approach was proposed to determine the optimal disposition of FRP, relying into a final check of the increase of the load bearing capacity of the structure subsequent to the change of the failure mechanism. However, while limit analysis is a powerful and relatively simple tool, it does not provide any data on displacements at failure -an information required by many codes of practice in this specific field-, assumes for the constituent materials a rigid-perfectly plastic behavior with infinite ductility for the constituent materials, a hypothesis rather questionable in this case. The need of developing a fully non-linear model, capable of reproducing, with few variables and in an approximate but suitable way, the actual deteriorating behavior of both masonry and reinforcement appeared unavoidable. The passage from limit analysis to non-linear models came gradually and has been recently proposed for the analysis of small unreinforced masonry laboratory panels out-of-plane loaded. In particular, in Milani & Tralli (2011), a discretization with Munro and Da Fonseca rigid triangular elements with linear and non-linear deformation concentrated on interfaces exclusively for bending actions has been proposed. In this way, only two plastic multipliers per interface were required and the number of kinematic variables involved to perform full non-linear analysis was rather limited. In order to circumvent some typical drawbacks of standard FEM in the softening range, the non-linear problem was re-formulated within non-linear programming, by means of a Sequential Quadratic Programming scheme capable of following the non-linear pushover curve in the softening range.

From a numerical point of view, the choice of using rigid blocks with deformations lumped at interfaces in spite of standard FEs is essentially inspired by the need of variables reduction, but also reproduces the actual deformations pattern in the non-linear field at least for masonry with sufficiently regular texture, where usually damage propagates on small fracture lines, zigzagging along joints between adjacent bricks. This approach potentially allows to perform numerical simulations on entire medium/large scale structures at a fraction of the time required by standard FEs. The utilization of discrete elements has a long tradition in the mechanics of structures and basically goes back to the pioneering work proposed by Kawai (1978).

The utilization of rigid elements, a much reduced number of DOF and the efficiency of the procedure tested for unreinforced panels in two-way bending, suggested a further improvement of the non linear model, relying into its extension to in-plane loaded panels (Milani 2011) and its successive generalization to curved masonry shells (Milani & Tralli 2012). Several additional complications arose in this latter case, connected to the increase of variables to be handled per interface (modeled by means of five non-linear springs), the introduction of a simplified dependence between out-of-plane behavior and membrane internal actions and the utilization of more efficient large scale Quadratic Programming routines, to handle more realistic engineering problem and hence much more elements in the FE discretization. The approach presented in this paper should be seen as a further development of the non-linear model constituted by rigid wedge elements and non-linear interfaces firstly proposed in Milani & Tralli (2011), where (1) external reinforcement is introduced at a structural level and modeled by means of the utilization of plate and shell elements with deformation allows at the linear interfaces between adjoining elements and (2) a brittle 2D constitutive behavior between FRP and support is introduced, fully complying with codes of practice recommendations (e.g. CNR-DT 200 2004).

The use of advanced models for the assessment of existing masonry structures is necessary to adopt efficient conservation and strengthening measures, to develop better design tools and to partly replace the expensive laboratory tests.

3. Meso-scale: a simplified homogenization procedure

A simplified homogenization model for the determination of non-strengthened macroscopic masonry non-linear behavior is presented first. The homogenization proposed (Milani et al. 2009a) pertains to running bond non-strengthened masonry, regarded as an assemblage of bricks interacting through interfaces (mortar joints). Bricks are supposed infinitely resistant, whereas for joints a Mohr Coulomb failure criterion with tension cut-off and compressive limited strength is adopted. In this way, a full description of the model can be given at a *micro-scale* considering a representative volume constituted by a generic brick interacting with its six neighbors. A sub-class of possible elementary deformation modes acting in the unit cell is a priori chosen in order to describe joints cracking under normal, tangential actions and bending. Then, a numerical procedure of identification between the 3D discrete system and a continuum 2D equivalent model is proposed, equating internal work expended by the two models.

3.1. Heterogeneous model

In the heterogeneous model, the whole REV is meshed through six-noded wedge elements interconnected by interfaces (internal brick-brick interfaces and mortar joints, see Figure 2-a). The motion of a generic element E, see Figure 2, is described as a function of its centroid (C^E) displacement vector $\mathbf{u}^E$ (components u_{xx}^E, u_{yy}^E and u_{zz}^E) and of its rotation vector $\mathbf{\Phi}^E$ (components Φ_{xx}^E, Φ_{yy}^E and Φ_{zz}^E) around centroid.

When two contiguous bricks M and N are considered, the displacement of a generic point P in a position $\boldsymbol{\xi} \in \Gamma_{12}$ belonging respectively to M and N (where Γ_{12} indicates the common interface between the two elements) is:

$$\mathbf{u}^M(P) = \mathbf{u}^M + \mathbf{M}(\mathbf{\Phi}^M)(P - C^M)$$

$$\mathbf{u}^N(P) = \mathbf{u}^N + \mathbf{M}(\mathbf{\Phi}^N)(P - C^N) \tag{1}$$

Where $\mathbf{M}(\mathbf{\Phi}) = = \begin{bmatrix} 0 & -\Phi_{zz} & \Phi_{yy} \\ \Phi_{zz} & 0 & -\Phi_{xx} \\ -\Phi_{yy} & \Phi_{xx} & 0 \end{bmatrix}$

In equation (1) the position $\boldsymbol{\xi}$ of point P is evaluated with reference to a local frame of reference $(\xi_1 \ \ \xi_2)$ with origin on the centroid on the interface, Figure 2-b. Jump of displacements $[\mathbf{U}(P)]$ between bricks M and N in a point $\boldsymbol{\xi} \in \Gamma_{12}$ is expressed by:

$$\lfloor \mathbf{U}(P) \rfloor = \mathbf{u}^M(P) - \mathbf{u}^N(P) = \mathbf{u}^M - \mathbf{u}^N + \mathbf{M}(\mathbf{\Phi}^M)(P - C^M) - \mathbf{M}(\mathbf{\Phi}^N)(P - C^N) \tag{2}$$

Having defined a local frame of reference ξ_1-ξ_2-ξ_3 for the interface between N and M elements (vertices corresponding to nodes P_1, P_2, P_4 and P_5, Figure 2-b and -c), we assume that it is characterized by two axes ($\mathbf{e}_1$-$\mathbf{e}_2$) laying on the interface plane and mutually orthogonal, while the third perpendicular axis to the interface is $\mathbf{e}_3$. Thus, unitary vectors $\mathbf{e}_1$-$\mathbf{e}_2$-$\mathbf{e}_3$ may be expressed in the global coordinate system as $\mathbf{e}_1 = \mathbf{e}_2 \times \mathbf{e}_3$, $\mathbf{e}_2 = \dfrac{P_2 - P_1}{\|P_2 - P_1\|}$ and $\mathbf{e}_3 = \tilde{\mathbf{e}}_1 \times \mathbf{e}_2$ with $\tilde{\mathbf{e}}_1 = \dfrac{P_4 - P_1}{\|P_4 - P_1\|}$.

The rotation matrix $\mathbf{R}_\mathbf{e}$, with respect to the global coordinate system jump of displacements, may be written in the local system as:

$$[\tilde{\mathbf{U}}(P)] = \mathbf{R}_\mathbf{e}[\mathbf{U}(P)] \tag{3}$$

where the superscript ˜ indicates quantities evaluated in the local system.

From (3), it is possible to evaluate the work π dissipated on Γ_{12} as follows:

$$\pi = \int_I [\boldsymbol{\sigma}_M(P) \cdot \tilde{\mathbf{U}}_M(P) + \boldsymbol{\sigma}_N(P) \cdot \tilde{\mathbf{U}}_N(P)] dS = \int_I \boldsymbol{\sigma}_M(P) \cdot [\tilde{\mathbf{U}}(P)] dS \tag{4}$$

Where $\boldsymbol{\sigma}_M(P) = [\tau_{13}(P) \ \tau_{23}(P) \ \sigma_{33}(P)]^T$ is the stress vector acting at P on element M, with $\boldsymbol{\sigma}_N(P) = -\boldsymbol{\sigma}_M(P)$.

3.2. Continuous model

In this Section, with the aim of substituting, for the structural analyses, the heterogeneous material with an equivalent homogenized continuum, the basic kinematics of an equivalent model is discussed. In particular, a standard Cauchy bi-dimensional continuum, Figure 2-a, is considered. Here the global frame of reference is identified by the vectors x_1, x_2 and x_3.

The displacement field of a point $\mathbf{P}$ (coordinates $\left[x_1^P \quad x_2^P \quad x_3^P\right]$) belonging to the equivalent continuum plate is given by fields $\mathbf{w}(\mathbf{x})$ (components w_1, w_2 and w_3) and $\mathbf{\Psi}(\mathbf{x})$ (components Ψ_1 and Ψ_2), representing respectively the displacements and rotations of the plate in correspondence of the point $\mathbf{x} = \left[x_1^P \quad x_2^P \quad 0\right]$ laying in the middle plane of the continuum regarded as a plate (i.e. with two dimensions much bigger than a third one, the thickness).

For in- and out-of-plane loads, membrane forces vector N (components N_{11}, N_{12} and N_{22}), moments M (bending M_{11}, M_{22} and torsion M_{12}) and out-of-plane shear $\mathbf{T}$ (components T_{13} and T_{23}) contribute to the internal work. In particular, the work dissipated by an equivalent plate model is simply:

$$\pi = \left[N_{11} \quad N_{12} \quad N_{22}\right]\begin{bmatrix} E_{11} \\ E_{12}+E_{21} \\ E_{22} \end{bmatrix} + \left[T_{13} \quad T_{23}\right]\begin{bmatrix} \gamma_{13} \\ \gamma_{23} \end{bmatrix} + \left[M_{11} \quad M_{12} \quad M_{22}\right]\begin{bmatrix} \chi_{11} \\ \chi_{12}+\chi_{21} \\ \chi_{22} \end{bmatrix} \tag{5}$$

where $\mathbf{E}$ is the in-plane strain vector, $\boldsymbol{\chi}$ the out-of-plane strain vector and $\boldsymbol{\gamma}$ the out-of-plane shear strain.

3.3.Simplified homogenization

To substitute the heterogeneous material with the homogeneous equivalent 2D model, a simple compatible identification model is proposed (Casolo & Milani 2010), where the work expended by the blocks model, equation (4), is equated to the work (5) by the equivalent model.

At this aim, fields $\mathbf{w}(\mathbf{x})$ and $\mathbf{\Psi}(\mathbf{x})$ are a priori chosen as a combination of elementary deformations in the unit cell, corresponding to actual failure mechanisms occurring, according to experimental evidences, in presence of running bond brickwork with weak joints reduced to interfaces. From a practical point of view, fields $\mathbf{w}(\mathbf{x})$ and $\mathbf{\Psi}(\mathbf{x})$ corresponding to each sub-class of regular motions are obtained assuming alternatively one component of vector $\mathbf{E}$, $\boldsymbol{\gamma}$ or $\boldsymbol{\chi}$ unitary and setting all the other components equal to zero, subsequently choosing the most simple polynomial expressions for $\mathbf{w}(\mathbf{x})$ and $\mathbf{\Psi}(\mathbf{x})$ which comply with the compatibility equations. Once fields $\mathbf{w}(\mathbf{x})$ and $\mathbf{\Psi}(\mathbf{x})$ are known from the procedure described, rotations and displacements of each element belonging to the REV in the heterogeneous model are determined solving a boundary value problem on the REV where displacements (or displacement increments) on the boundary are imposed.

For instance, when only $\chi_{11} \neq 0$ is applied on the REV, a choice for $\mathbf{w}(\mathbf{x})$ and $\mathbf{\Psi}(\mathbf{x})$ fields is:

$$\Psi_1 = \chi_{11} x_1$$

$$\begin{aligned} w_1 &= \chi_{11} x_1 x_3 \\ w_2 &= 0 \\ w_3 &= -\chi_{11} x_1^2 / 2 \end{aligned} \qquad (6)$$

The application of equation (6) to the heterogeneous model permits to directly determine displacements to apply to the boundary surfaces of the REV.

Since the aim of this paper is to model the strengthening effect induced by FRP in bending, at the macro-scale homogenized three dimensional wedge-shaped elements are used for masonry (see following sections and Figure 1). Consequently, non-strengthened brickwork behavior in flexion is obtained by integration of in plane actions at a structural level (step II).

Therefore, at the micro-scale it is possible to limit the study to in-plane and out-of-plane shear actions ($\mathbf{E}$, $\boldsymbol{\gamma}$ respectively).

For a generic brick-brick or mortar interface, the elastic domain is, in the most general case, bounded by a composite yield surface that includes tension, shear and compression failure with softening, Figure 2-d. A multi-surface plasticity model is adopted, with softening in both tension and compression. The elastic domain is defined by each i-th yield function $f_i \leq 0$, in the form $f_i(\sigma,\tau,\kappa_i) = \Phi_i(\sigma,\tau) + \Psi_i(\kappa_i)$, where scalar κ_i rules the amount of softening of the i-th yield surface and Φ_i and Ψ_i are generic functions representing respectively the initial i-th yield surface and the correction which accounts for the evolution of the strength during the inelastic deformation process. Total strain rate $\dot{\boldsymbol{\varepsilon}}$ is decomposed into an elastic component $\dot{\boldsymbol{\varepsilon}}_{el}$ and a plastic component $\dot{\boldsymbol{\varepsilon}}_{pl}$. The elastic strain rate is related to the stress rate by the elastic constitutive matrix D as $\dot{\boldsymbol{\sigma}} = \mathbf{D}\dot{\boldsymbol{\varepsilon}}_{el}$, whereas the non-associated plasticity reads as $\dot{\boldsymbol{\varepsilon}}_{pl} = \lambda_i \frac{\partial g_i}{\partial \boldsymbol{\sigma}}$, where g_i is the plastic potential corresponding to the i-th yield surface (which rules the direction of $\dot{\boldsymbol{\varepsilon}}_{pl}$ in the stress space) and $\boldsymbol{\sigma} = [\sigma \quad \tau]^T$.

The multi-surface plasticity model adopted is the classical Mohr–Coulomb type strength criterion, with a tension cut-off and a linear compression cap, Figure 2-d. f_t and f_c are, respectively, tensile and compressive Mode-I strength, c is the cohesion, Φ is the friction angle, and Ψ is the angle which defines the linear compression cap. For the tension mode, exponential softening is assumed, i.e. $f_1(\boldsymbol{\sigma},\kappa_1) = \sigma - f_t(\kappa_1)$. where $f_t(\kappa_1)$ deteriorates in agreement with the following formula:

$$f_t(\kappa_1) = f_{t0} e^{-\frac{f_{t0}}{G_f^I}\kappa_1} \tag{7}$$

being f_{t0} the initial joint tensile strength and G_f^I the mode I fracture energy. An associated flow rule is assumed. For the shear mode, the Mohr-Coulomb yield function reads $f_2(\boldsymbol{\sigma},\kappa_2) = |\tau| + \sigma \tan\phi(\kappa_2) - c(\kappa_2)$, where the yield values c and $\tan\phi$ are ruled by the following formulas:

$$\begin{aligned} c(\kappa_2) &= c_0 e^{-\frac{c_0}{G_f^{II}}\kappa_2} \\ \tan\phi &= \tan\phi_0 + (\tan\phi_r - \tan\phi_0)(c_0 - c)/c_0 \end{aligned} \tag{8}$$

being c_0 and $\tan\phi_0$ the initial cohesion and friction angle, G_f^{II} the mode II fracture energy and $\tan\phi_r$ the residual friction angle, here kept always equal to 75% of the initial one. A non-associated flow rule is assumed here, with zero dilatancy.

When dealing with the linearized compressive cap inelastic behavior, a three function model, Lourenço and Rots (1997), is utilized as shown in Figure 2-d, where the subscripts *e*, *m*, *p* and *r* of the yield value f_c denote respectively, the elastic limit, medium, peak and residual values. The peak value f_{cp} equals the masonry compressive strength f_c of the interface. Stress within the hardening/softening evolution is evaluated by means of the following formulas:

$$\begin{aligned}
\sigma_I(\kappa_3) &= f_{ce} + \left(f_{cp} - f_{ce}\right)\sqrt{2\frac{\kappa_3}{\kappa_p} - \left(\frac{\kappa_3}{\kappa_p}\right)^2} \\
\sigma_{II}(\kappa_3) &= f_{cp} + \left(f_{cm} - f_{cp}\right)\left(\frac{\kappa_3 - \kappa_p}{\kappa_m - \kappa_p}\right)^2 \\
\sigma_{III}(\kappa_3) &= f_{cr} + \left(f_{cm} - f_{cr}\right)\exp\left(2\frac{f_{cm} - f_{cp}}{\kappa_m - \kappa_p}\frac{\kappa_3 - \kappa_p}{f_{cm} - f_{cr}}\right)
\end{aligned} \tag{9}$$

3.4. Numerical simulations at a cell level

This section provides an insight into the inelastic behavior of masonry REVs with any shape, provided by the two-step model proposed.

To this aim, a running bond elementary cell constituted by ¼ of common solid clay Italian bricks (dimensions 62.5 × 30 × 14 mm) is considered and is utilized to build some FRP strengthened deep beams analyzed in Part II (Grande et al. 2008). Elastic and inelastic material properties are summarized in Table I. Two different values of fracture energy G_I are assumed, the first corresponding realistically to existing masonry (Case A), the second assuming an almost perfect plastic behavior in tension (Case B). FE discretization adopted is sketched in Figure 3-a. The behavior in uniaxial tension is depicted in Figure 4-a for horizontal and vertical tension. The anisotropy of the homogenized model is particularly evident and is mainly due to the contribution in horizontal tension of the bed joint, which fails in shear. In order to validate the results, the curves obtained using classic FE simulation (Pegon & Anthoine 1997) performed on a mesh with 384 elastic plane stress quadrilateral elements and mortar elasto-plastic interfaces are also represented, indicated as “FEM refined mesh”. As it is possible to notice, the agreement is almost perfect, even in the softening range. This is not surprising because fracture lines concentrates on joints reduced to interfaces, as demonstrated by the REV deformed shape depicted in Figure 4-b, where normal stress-shear masonry interfaces damage maps are also reported for the sake of completeness. A very similar behavior is experienced in horizontal bending, as can be noted by deformed shape and interfaces damage patch reported in Figure 4-c. For compression loads, the anisotropy is less evident, due to the low shear strength of the joint when compared to the compressive strength. Hence, little differences are expected when comparing the horizontal and vertical compression. For this reason, in Figure 5-a only the behavior of the cell in vertical compression is represented for the sake of conciseness, along with 4 approximations (of increasing accuracy) obtained with linear piecewise constant functions, to use at a structural level (Part II). To be predictive in compression, a model with damage inside elements bulk can be used, Fedele & Milani (2010) even if more complex models seem to be needed, Lourenço & Pina-Henriques (2006). Still, anisotropy and actual masonry compression strength may be easily fitted with the model proposed, assuming different mechanical properties for vertical and horizontal joints.

Finally, in Figure 5-b, the pure shear behavior of the REV is represented at three increasing vertical values of pre-compression. As expected, both peak strength and ductility increase; once again in reasonable agreement with available experimental data and proposed numerical models, Lourenço & Rots (1997) and Lotfi & Shing (1994).

The second REV analyzed, again to be used in Part II structural analyses, is a curved cell constituting a circular arch studied by Mahini et al. (2007), see Figure 3-b for the FE discretization here adopted. The middle plane of the wall is also represented to highlight the curvature of the REV.

Mechanical properties adopted for constituent materials are summarized in Table II and, where available, correspond to Mahini et al. (2007) values. In particular, in Mahini et al. (2007), a wide experimental characterization in compression of brick prisms extracted from the original units as a part of the vaults is at disposal, with full force-displacement diagrams. Each prism was made of seven solid clay bricks and thick mortar joints. An experimental characterization of the ultimate tensile strength is also available, to compare with present model predictions for axial tensile actions. The behavior in uniaxial compression is depicted in Figure 6-a, where also experimental data and the numerical model by Mahini et al. (2007) are reported.

As can be noted, the agreement with experimental data is very satisfactory. The same simulations are repeated in tension, along both material axes. Stress-strain resultant curves are depicted in Figure 6-b. Here only a comparison between present results and experimental data available on the peak strength is possible. However, the general non-linear behavior of the REV seems reasonable and in agreement with literature data. When the REV is subjected to pure stretching acting along y1, see Figure 1 for symbol meaning, blocks tend to rotate around vertical axis y2, with a small but non negligible contribution, similarly to what occurs for a flat REV in bending, see Figure 4. The out-of-plane movement of the blocks tends also to slightly reduce the peak strength for stretching along y2, which, for the flat case, turns out to be equal to joints tensile strength.

Since the determination of the flexural non-linear behavior is crucial for a REV belonging to a masonry arch (which typically fails with the formation of cylindrical hinges under a certain level of axial pre-compression), the out-of-plane behavior of the REV is finally represented in Figure 7. In particular, Figure 7-a and -b show respectively the meridian and parallel curvature-bending moment diagrams computed by considering increasing values of the membrane meridian compression load N_{11} (see also Figure 3-b for local axes schematization). N_{11} has been varied in a wide range from zero to a reasonable value of compression. For the sake of completeness, in Figure 7-c the torsional behavior of the homogenized material is also represented under increasing membrane vertical compression loads.

Considering the flexural response results, the following aspects are worth noting:

- the largest flexural strength of masonry is obtained when loaded along a meridian hinge, which is due to the contribution of the bed joint subjected to tangential actions;
- the anisotropic character of the softening exhibited by the model after the peak strength, again a consequence of the role played by the bed joints;
- the stability of the algorithm, also in the post peak regime, essentially due to the very limited number of variables needed by the numerical model.

Deformed shapes obtained at the end of the simulations for a meridian bending moment and for torsion (in absence of meridian pre-compression) are finally reported in Figure 8-b and -c for the sake of completeness.

3.5. 3-noded flat FRP elements (triangles)

At a structural level, rigid triangular shell elements are used to model FRP, Figure 9. Being rigid, elastic and inelastic deformation is allowed only at the interfaces between contiguous elements.

Let us consider a (k)-th FRP strip with direction $\mathbf{s}^{(k)}$ and two contiguous FRP elements M and N, with centroid displacements and rotations defined as $\mathbf{u}^M = \left[u_{xx}^M \ \ u_{yy}^M \ \ u_{zz}^M\right]^T$, $\mathbf{u}^N = \left[u_{xx}^N \ \ u_{yy}^N \ \ u_{zz}^N\right]^T$, $\mathbf{\Phi}^M = \left[\Phi_{xx}^M \ \ \Phi_{yy}^M \ \ \Phi_{zz}^M\right]^T$ and $\mathbf{\Phi}^N = \left[\Phi_{xx}^N \ \ \Phi_{yy}^N \ \ \Phi_{zz}^N\right]^T$. Jump of displacements on the common M and N interface ($I-FRP$) is linear: therefore, its evaluation is only necessary on the interface extremes A and B, calculated as the difference between displacements of nodes 1-3 and 2-4 respectively.

Furthermore, a local frame of reference $\mathbf{s}^{(k)}$-$\mathbf{t}^{(k)}$-$\mathbf{r}^{(k)}$ has to be defined on the interface as (see also Figure 9 for symbols meaning):

$$\begin{cases} \mathbf{s}^{(k)} = \dfrac{(P_7 - P_5) + (P_6 - P_8)}{\left\| (P_7 - P_5) + (P_6 - P_8) \right\|} \\ \mathbf{t}^{(k)} = \mathbf{r}^{(k)} \times \mathbf{s}^{(k)} \\ \mathbf{r}^{(k)} = \dfrac{\mathbf{r}^M + \mathbf{r}^N}{\left\| \mathbf{r}^M + \mathbf{r}^N \right\|} \end{cases} \qquad (10)$$

Where $\mathbf{r}^{(M)} = \dfrac{(P_1 - P_5) \times (P_2 - P_5)}{2A_{125}}$ and $\mathbf{r}^{(N)} = \dfrac{(P_4 - P_6) + (P_3 - P_6)}{2A_{346}}$, having defined A_{125} and A_{346} as the areas of elements M and N respectively.

Being $[x_A \ \ y_A \ \ z_A]$ point A coordinates, the node 1 displacement is given by:

$$\begin{bmatrix} u_{xx}^1 \\ u_{yy}^1 \\ u_{zz}^1 \end{bmatrix} = \begin{bmatrix} u_{xx}^M \\ u_{yy}^M \\ u_{zz}^M \end{bmatrix} + \begin{bmatrix} 0 & \Phi_{yy}^M & -\Phi_{zz}^M \\ -\Phi_{yy}^M & 0 & -\Phi_{xx}^M \\ -\Phi_{zz}^M & \Phi_{xx}^M & 0 \end{bmatrix} \begin{bmatrix} x_A - x_M \\ y_A - y_M \\ z_A - z_M \end{bmatrix} = \mathbf{u}^M + \mathbf{R}_M \left(A - C^M\right) \qquad (11)$$

Where $C^M = [x_M \quad y_M \quad z_M]$ is the centroid of element M.

The node 1 displacement can be re-written in the $\mathbf{s}^{(k)}$-$\mathbf{t}^{(k)}$-$\mathbf{r}^{(k)}$ local interface frame of reference by means of the rotation matrix $\mathbf{T}(M, N)$ deduced from equations (11), i.e. $[u_s^1 \quad u_r^1 \quad u_t^1]^T = \mathbf{T}(M, N)\left[\mathbf{u}^M + \mathbf{R}_M \left(A - C^M\right)\right]$. No difference occurs for node 2, provided that element N displacements and centroid are used instead of quantities related to M.

Consequently, A jump of displacements is evaluated (in the local coordinate system) as:

$$[\mathbf{u}_A] = \mathbf{T}(M, N)\left[\mathbf{u}^M - \mathbf{u}^N + \mathbf{R}_M \left(A - C^M\right) - \mathbf{R}_N \left(A - C^N\right)\right] \qquad (12)$$

Where $[\mathbf{u}_A] = \left[\Delta u_s^A \ \ \Delta u_r^A \ \ \Delta u_t^A\right]^T = \left[u_s^1 - u_s^2 \ \ u_r^1 - u_r^2 \ \ u_t^1 - u_t^2\right]^T$ is the jump of displacement on A. Analogous considerations can be repeated for node B.

As already discussed, elastic and inelastic deformation is supposed to occur at the interfaces only, due to stresses acting both parallel and perpendicular to $\mathbf{s}^{(k)}$ fibers direction. Low compressive stresses induce buckling of the strips, due to the FRP negligible thickness. In order to take into account this effect (at least in an approximate way), different limit stresses are assumed in tension and compression, namely f_{FRP}^{+} (assumed equal to f_{fdd} or $f_{fdd,rid}$ in agreement with CNR-DT200

(2004), see following section) for tensile failure and $f_{FRP}^{-} \approx 0$ for compression buckling respectively.

3.6. FRP/masonry interfaces (delamination)

A key parameter for FRP strengthening is the adhesion between the strip and masonry. In particular, delamination is very complex to model, because it involves materials with different properties (masonry, FRP and glue layer) and depends on several parameters. Experimental and numerical studies demonstrated that decohesion usually occurs for masonry failure (Fedele and Milani 2010), i.e. delaminated FRP presents a significant layer of masonry material on the debonded surface.

A rigorous methodology to directly take into account in a numerical model the behavior of the layer between masonry and FRP requires the use of the interface model concept. According to this model, forces acting on the interface are related to the relative displacement of the two sides (masonry and FRP), thus requiring the utilization of interface elements.

For the sake of simplicity, in what follows, the Italian code CNR DT-200 (2004) is used next, which is one of the many national codes proposed in this field. Anyway, it is stressed that any formula may be implemented in the code with no conceptual differences.

In the Italian norm, Figure 9-a, a simplified approach is proposed to evaluate the delamination phenomenon, suitably limiting force action on the FRP strip. In particular, the f_{fdd} design tensile strength of FRP elements is:

$$f_{fdd} = \frac{1}{\gamma_{fd}\sqrt{\gamma_M}}\sqrt{\frac{2 \cdot E_{FRP} \cdot \Gamma_{Fk}}{t_{FRP}}} \qquad (13)$$

if the so called bond length l_b is greater than the optimal bond length l_e or:

$$f_{fdd,rid} = f_{fdd}\frac{l_b}{l_e}\left(2 - \frac{l_b}{l_e}\right) \qquad (14)$$

if $l_b \le l_e$.

$f_{fdd,rid}$ is the reduced value of the design bond strength, f_{fdd} is the design bond strength, E_{FRP} is the FRP Young modulus, t_{FRP} is the FRP thickness, γ_{fd} and γ_M are safety factors (in what follows assumed equal to 1.20 and 1.0 respectively), l_b is the bond length of FRP elements and $l_e = \sqrt{\frac{E_{FRP} \cdot t_{FRP}}{2 \cdot f_{mtm}}}$ is the optimal bond length of FRP corresponding to the minimal bond length able to carry the maximum anchorage force (f_{mtm} indicates masonry average tensile strength).

The term Γ_{Fk} in (13) represents the characteristic value of the specific fracture energy of the FRP strengthened masonry under a delamination test. Γ_{Fd} (design value) may be evaluated as follows:

$$\Gamma_{Fd} = c_1 \sqrt{f_{mk} \cdot f_{mtm}} \quad [f \ in \ N/mm^2] \tag{15}$$

where c_1 is an experimentally determined coefficient, that typically ranges between 0.015÷0.030 and f_{mk} is the characteristic value of masonry compressive strength.

The τ_b (interface shear stress)-slip law proposed by the Italian norm, Figure 9, permits an indirect evaluation of shear peak stress (here denoted with the symbol f_b) to use for masonry/FRP interface elements (and thus avoiding a discretization of FRP strips by means of truss elements with limited strength f_{fdd}), once that the ultimate slip (usually fixed at 0.3 mm) is known (area under the τ_b-slip constitutive law of Figure 9 is Γ_{Fd}).

For a triangular FRP-masonry interface I^{F-M} between elements F (FRP) and M (masonry), Figure 9, $\mathbf{u}^F = \left[u_{xx}^F \ u_{yy}^F \ u_{zz}^F\right]^T$ and $\mathbf{u}^M = \left[u_{xx}^M \ u_{yy}^M \ u_{zz}^M\right]^T$ indicate F and M centroids displacements respectively, whereas $\mathbf{\Phi}^F = \left[\Phi_{xx}^F \ \Phi_{yy}^F \ \Phi_{zz}^F\right]^T$ and $\mathbf{\Phi}^M = \left[\Phi_{xx}^M \ \Phi_{yy}^M \ \Phi_{zz}^M\right]^T$ F and M rotation vectors. Jump of displacements on the common I^{F-M} interface is linear and may be evaluated on nodes A, B and C of the interface (Figure 9) as difference between displacements of nodes 1-4 and 2-5 and 3-6 respectively. In particular, if $\left[x_A \ y_A \ z_A\right]$ represents point A coordinates, displacement of node 1 is again given by an equation formally identical to (11).

For I^{F-M}, we introduce the same $\mathbf{s}^{(k)}$-$\mathbf{t}^{(k)}$-$\mathbf{r}^{(k)}$ local frame of reference defined in equation (10) (see also Figure 9-c), useful to re-write the jump of displacement in a local frame.

For node A belonging to I^{F-M} and connecting nodes 1-4, it is necessary to evaluate the displacement field of node 1 (masonry) and 4 (FRP) in the local frame of reference using the same formula reported in (12). In this way, jump of displacements on A (in the local coordinate system) may be evaluated as:

$$[\mathbf{u}_A] = \mathbf{T}(M, N)\left[\mathbf{u}^M - \mathbf{u}^N + \mathbf{R}_M\left(A - C^M\right) - \mathbf{R}_N\left(A - C^N\right)\right] \tag{16}$$

Where $[\mathbf{u}_A] = \left[\Delta u_s^A \quad \Delta u_r^A \quad \Delta u_t^A\right]^T = \left[u_s^1 - u_s^4 \quad u_r^1 - u_r^4 \quad u_t^1 - u_t^4\right]^T$ is called "slip" vector of the interface on *A*. No conceptual differences occur for nodes B and C, therefore equation (16) can be utilized for all the vertices of the triangular interface.

In the present model, a linear piecewise constant approximation of the actual relationship between slip components (Δu_r^A and Δu_t^A) -tangential stresses (τ_r and τ_t) is adopted, to handle delamination phenomenon in the framework of quadratic programming, as discussed in detail in the following section. The actual elasto-damaging behavior of the interface is approximated with the function depicted in Figure 9-a. Δu_s^A is assumed exclusively elastic, in absence of consolidated experimental evidences describing the interfacial behavior for normal stresses.

4. Macro-scale (structural level): a simple sequential quadratic programming –SQP– approach

The kinematic meso-scale model proposed allows to obtain masonry stress-strain diagrams at different orientations of load with respect to material axis. The out-of-plane behavior may be reproduced as well. However, since six-noded wedge elements are used at a structural level, interfaces are subdivided into small rectangular areas and macroscopic internal actions N, T, M are obtained by integration of stress-strain curves evaluated on the REV. For this reason, only the average membrane behavior (normal stress-normal strain and two mutually orthogonal tangential stress-tangential deformation curves for each interface) is required at the macro-scale.

The elastic plastic response of a structure subjected to given proportionally increased loads is given by the following set of equations and inequalities (De Donato & Franchi 1973):

$$\begin{cases} \boldsymbol{\varepsilon}^{plE} = \mathbf{N}^E \boldsymbol{\lambda}^E \\ \boldsymbol{\Phi}^E = \left(\mathbf{N}^E\right)^T \boldsymbol{\sigma} - \mathbf{H}^E \boldsymbol{\lambda}^E \\ \boldsymbol{\Phi}^E \leq 0 \quad \boldsymbol{\lambda}^E \geq \mathbf{0} \\ \boldsymbol{\lambda}^E \boldsymbol{\Phi}^E = 0 \end{cases} \tag{17}$$

where, in the general context of a finite element discretization of the domain:

1. $\boldsymbol{\varepsilon}^{plE}$ is the plastic strain vector of the element E;
2. $\mathbf{N}^E$ is the shape functions matrix of the used finite element;
3. $\boldsymbol{\lambda}^E$ is the plastic multiplier vector;
4. $\mathbf{H}^E$ is the hardening matrix, which in this case is diagonal and with non-null values, very small with the aim of reproducing the elastic-perfectly plastic case;
5. $\boldsymbol{\Phi}^E$ is a vector collecting the r linearization planes of the failure surface.
6. $\boldsymbol{\sigma}$ is the vector of stress parameters which define point by point the stress (or internal actions) acting on the finite element.

Hypotheses assumed are: (1) the plasticity condition is piecewise-linearized with *r* linearly elastic-plastic interacting planes in the space of superimposed stress and strain components; (2) unloading of yielded stress-points does not occur; (3) the continuum is discretized into constant strain and stress finite elements.

Alternatively, De Donato & Franchi (1973), the solution of (17) can be achieved using quadratic programming:

$$\begin{cases} \max\left\{-\frac{1}{2}\left(\boldsymbol{\lambda}^E\right)^T \mathbf{H}^E \boldsymbol{\lambda}^E + \left(\boldsymbol{\lambda}^E\right)^T \left(\mathbf{N}^E\right)^T \mathbf{D}^E \boldsymbol{\varepsilon}^E \right. \\ \qquad \textit{subject to}: \boldsymbol{\lambda}^E \geq \mathbf{0} \end{cases} \tag{18}$$

where $\mathbf{D}^E$ is the elastic stiffness matrix, $\boldsymbol{\varepsilon}^E$ is the elastic part of the strain vector and all the other symbols have been already introduced.

As already discussed, the finite element model utilized next to analyze in the non-linear range masonry vaults relies into a discretization through six-noded wedge elements, assumed rigid infinitely resistant, and quadrilateral interfaces where all deformation occurs (linear and non-linear). They are constituted by homogenized masonry, FRP interfaces and masonry-FRP bond. No differences occur with the procedure adopted at a cell level except that (1) for all interfaces an approximation of the non-linear behavior through a linear piecewise constant function is used and (2) masonry interfaces stress-strain curves depend exclusively on the orientation of the interfaces.

With the aim of suitably reproducing out-of-plane behavior of the interfaces, a relatively refined subdivision of interfaces along the thickness is adopted (typically 10 layers are used). In this way, bending moment and torsion may be evaluated step by step during the deformation process simply by integration along the thickness.

When dealing with masonry material, three displacement and two rotational non linear springs are utilized, as schematically shown in Figure 10. The third rotational spring, acting along an axis parallel to the surface, is assumed rigid and infinitely resistant. For FRP-masonry interfaces, three displacement springs per node are assumed.

To properly take into account some distinctive aspect of masonry behavior in flexion (dependence of the flexural behavior by in-plane compression), but limiting to a great extent the number of optimization variables involved in the QP scheme, the procedure envisaged in Figure 10 is adopted for each interface.

Focusing for the sake of brevity exclusively on bending moment acting on an interface *k* (a similar procedure is adopted to handle torsion), at an iteration (i) of the loading process, bending rotation $\Phi_n^{(i-1)}$ and normal displacement of the interface centroid $\delta_n^{(i-1)}$ of the previous iteration (i-1) are known. It is therefore immediately known the displacement field $\delta_n\left(y_{t2}\right)$ along the interface thickness (abscissa y_{t2}). For each interface, depending on its orientation with respect to blocks disposition, the homogenized stress-strain behavior is known from the meso-scale. At each assumed strain ε_n, an interface displacement at the macro-scale is univocally associated simply applying what stated in Kawai (1978). In particular, given ε_n, the corresponding displacement in the discrete model on the interface k between elements M and N is $\delta_n = 1/2\left(V_M^I + V_N^I\right)/A^I \varepsilon_n$, where all symbols are graphically explained in Figure 10.

For the interface k the homogenized stress-displacement relationship is therefore known for each point of the interface. By integration with a reasonable subdivision along the thickness into layers (authors experienced that the utilization of 10 layers represents a good compromise between numerical efficiency and accuracy) the compression load $N^{(i-1)}$ on the interface at the (i-1)-th iteration is known. At a fixed value of membrane normal force, the non-linear relationship moment-curvature is known again from the meso-scale, along with its linear stepwise constant approximation (necessary to use the sequential quadratic programming scheme discussed in the sequel). Again the passage between curvatures and rotations, necessary when a discrete representation at a structural level is adopted, is trivial and again due to Kawai (1978).

In this way, bending moment and torsion may be evaluated step by step during the deformation process simply by integration.

A database of moment-curvature diagrams at different levels of normal stresses is always at disposal from meso-scale computations before any structural non-linear simulation. When normal membrane force is within the range inspected but does not match exactly values investigated, a linear interpolation law for the diagrams is used. In order to utilize sequentially the QP approach an approximation of the non-linear behavior through a linear piecewise constant function is used.

Following this procedure, the resultant mechanical model for masonry interfaces is thus composed by 5 elasto-plastic springs, Figure 10. Within each iteration, an elastic-perfectly plastic approximation for each spring is utilized, meaning that 10 plastic multipliers (two for each spring,

λ^+ and λ^-, corresponding to positive or negative kinematic variables) for each interface are needed. Conversely, for FRP masonry interfaces a total of 18 plastic multipliers are needed.

Within the FE model adopted, problem (18) may be re-written here (rigid elements with elastic-plastic interfaces) as follows:

$$\begin{cases} \min\left\{\frac{1}{2}\left[\left(\boldsymbol{\lambda}^+ - \boldsymbol{\lambda}^-\right)^T \mathbf{K}_{ep}\left(\boldsymbol{\lambda}^+ - \boldsymbol{\lambda}^-\right) + \mathbf{U}_{el}^T \mathbf{K}_{el} \mathbf{U}_{el}\right] - \mathbf{F}^T \mathbf{w}\right. \\ \qquad\qquad subject\ to : \boldsymbol{\lambda}^+ \geq \mathbf{0} \quad \text{and} \quad \boldsymbol{\lambda}^- \geq \mathbf{0} \end{cases} \qquad (19)$$

Assuming that the structural model has n_{el} elements, symbols in equation (19) have the following meaning:

1 $\mathbf{K}_{el}$ is a $6n_{el} \times 6n_{el}$ assembled diagonal matrix collecting elastic stiffness of each interface. It is worth remembering that elastic stiffness values are evaluated at the meso-scale, as discussed in the previous section. Since masonry is anisotropic both in the elastic and inelastic range, they depend on the interface orientation angle.

2. $\boldsymbol{\lambda}^+$ and $\boldsymbol{\lambda}^-$ are two vectors of plastic multipliers, collecting plastic multipliers of each non linear spring present in the model.

3. $\mathbf{K}_{ep}$ is the assembled diagonal matrix of hardening moduli of the interfaces. A small but nonzero hardening has to be introduced in order to avoid lack of convergence of the QP algorithm.

4. $\mathbf{U}_{el}$ is a $6n_{el}$ vector collecting the displacements and rotations of the elements.

5. $\mathbf{F}$ is a $6n_{el}$ vector of external loads (forces and moments) applied on element centroids.

Typically, the independent variable vector is represented by element displacements $\mathbf{U}_{el}$ and plastic multiplier vectors $\boldsymbol{\lambda}^+$ and $\boldsymbol{\lambda}^-$. Problem (19) is solved at increasing values of the external load vector $\mathbf{F}$ and, at each external load value, the initial trust independent variable vector is the solution at the previous step.

As usually done in a non-linear structural analysis, QP problem (19) is solved in terms of displacement and plastic multipliers step increments. The initial trust independent variable vector is always represented by the solution at the previous step.

In the framework of the two-step approach proposed, the actual stress-strain non-linear law of each spring representing masonry interfaces is at disposal at a structural level from the meso-scale (REV level). Since a softening behavior for joints is assumed, homogenized masonry exhibits softening too. Bricks staggering makes the resultant behavior of the interfaces also orthotropic. The non-linear stress-strain curve (both normal and shear behavior) is approximated using a linear-discontinuous piecewise constant function, as in Figure 5. Four approximations of increasing accuracy, obtained refining the number of steps utilized, are depicted. The drop of the load bearing capacity of the interfaces at increasing deformation is considered at a structural level. The possible strength deterioration of the material results in descending branches in the global load displacement curve of the structure. The following numerical procedure is used:

1. For all interfaces, an elastic-perfectly plastic law is assumed, which depends on the orientation of the interfaces (related to masonry anisotropy) and the level of deformation, i.e. jump of displacements of the interfaces. External loads are applied through small increments. The QP formulation (19) is used to estimate (i) rigid elements displacements and rotations and (ii) plastic multiplier vector $\boldsymbol{\lambda}^{+}$ and $\boldsymbol{\lambda}^{-}$ corresponding to the external load level considered.
2. At the very beginning, the structural response is all elastic, $\boldsymbol{\lambda}^{+}$ and $\boldsymbol{\lambda}^{-}$ are identically equal to zero. Increasing the external load results in yielding of one (or more) interfaces. A further increase of the external load vector is still possible, because of the possible contribution in stiffness and strength of the non- yielded interfaces. We assume that at the (*i*-1)-th load step the response of the structure on the pushover curve is represented by point A of Figure 11.
3. Step *i*. At the *i*-th load step, QP formulation (19) allows to estimate displacements $\mathbf{U}_{el}$ and plastic multiplier vectors corresponding to point B. However, differently to previous steps, we

assume that at least one plasticized interface (say *k*) reaches a strain value greater than $\varepsilon_{B'}$, see Figure 11, which bounds the drop of the strength of the interface *k* from N_I to N_{II}. We further assume, for the sake of simplicity but without loss of generality, that only *k* exhibits this load bearing capacity drop. In this case, the solution found at the *i*-th load step is inadmissible and does not represent the true response of the structure. Displacements $\mathbf{U}_{el}$ and plastic multipliers corresponding to point B' must be found. With this target in mind, a SQP approach is used, which is based on a bisectional procedure having, at the first sub iteration, as right and left extremes point A and B of the non-linear diagram. Here it is worth remembering that sequential methods of optimization have a wide tradition in structural engineering problems, see e.g. Cocchetti & Maier (2003), despite the fact that a multiplicity of solutions may in principle exist for non-convex problems (Kaliszky 1996, Denton & Morley 2000). Here, an engineering meaningful algorithm is proposed, which seems to converge realistically in the degradation range of the global force-displacement curve. At the first sub-iteration, $\mathbf{U}_{el}$, $\boldsymbol{\lambda}^{+}$ and $\boldsymbol{\lambda}^{-}$vectors corresponding to point P_1 standing in the middle of A and B are found solving QP problem (19) and assuming as starting point the solution available in A. Defined as $\Delta\mathbf{F}$ the external load vector increase passing from A to B, P_1 is the point representing the structural response of the structure corresponding to external load vector equal to $\mathbf{F}_A + \Delta\mathbf{F}/2$, being $\mathbf{F}_A$ the external load vector corresponding to A. Since $\mathbf{U}_{el}$, $\boldsymbol{\lambda}^{+}$ and $\boldsymbol{\lambda}^{-}$ are at disposal for P_1 solving (19), it is possible to establish if the strain of interface *k* in P_1 (ε_{P1}^{k}) exceeds $\varepsilon_{B'}$. If $\varepsilon_{P1}^{k} > \varepsilon_{B'}$ the search interval is bisected with extremes P_1 (left extreme) and B (right extreme), otherwise with A (left) and P_1 (right). $\mathbf{U}_{el}$, $\boldsymbol{\lambda}^{+}$ and $\boldsymbol{\lambda}^{-}$ are again evaluated in correspondence of the new middle point P_2 through QP (19). The procedure is iterated at the performer's discretion until $|\varepsilon_{Pj}^{k} - \varepsilon_{B'}|$<TOL, with TOL fixed tolerance. Here, it is worth underlining that the SQP procedure proposed is effective for small/medium scale QP problems and for approximations of the curvature-bending

moment diagrams with few (around 10-30) steps. However, this limitation seems acceptable for the analysis of entire masonry shells in combination with an averaging strategy (as the case here treated), which allows to limit considerably the computational effort.

4. Step (i+1) consists in evaluating $\mathbf{U}_{el}$, $\boldsymbol{\lambda}^{+}$ and $\boldsymbol{\lambda}^{-}$ in point C solving (19) and assuming as starting point B'. Firstly, the strength of the interface under consideration is decreased to C value. Then the QP problem is solved decreasing the external load until convergence of the algorithm is reached. Obviously, the matter within this step is the determination of the external load vector $\mathbf{F}_{B'} - \Delta\mathbf{F}_{C}$ to be applied to the structure. The choice is not unique but, to guarantee convergence of the algorithm, authors experienced that $\Delta\mathbf{F}_{C}$ may be found repeating some j sub-iterations assuming $\Delta\mathbf{F}_{C} = j\Delta\tilde{\mathbf{F}}_{C}$ where $\Delta\tilde{\mathbf{F}}_{C}$ is small enough (around 1/50-1/100 $\mathbf{F}_{B'}$). Again a bisectional approach between the un-converged and converged solution is utilized to bound closely C point, as done in step i, once a trial value with QP converged solution is found for $\Delta\mathbf{F}_{C}$.

5. Conclusions

In the present paper, the theoretical bases of a two-step FE software specifically developed for the analysis of FRP strengthened masonry structures have been presented. In the approach proposed, masonry macroscopic behavior is deduced in the first step, solving a non-linear boundary value problem on a suitable non-strengthened REV constituted by a central brick interconnected with its six neighbors by non-linear interfaces (mortar joints). In this way the macroscopic non-linear stress-strain behavior is estimated with a very limited computational effort. FRP is applied on the already homogenized material. At a structural level (step II), masonry is modeled with rigid wedge elements and non-linear homogenized interfaces, whereas for FRP rigid triangular elements bonded to the external masonry surface are used. Possible elastic and inelastic deformation on FRP is concentrated at the interfaces between adjoining elements. Delamination of the strip from the support is accounted for including in the model non-linear triangular interfaces between FRP and masonry. To handle complex non-linear problems with possible softening in a non-linear optimization framework, stress strain relationships for masonry, FRP and masonry/FRP bond are approximated with linear piecewise constant functions. Structural applications regarding flat and curved non-strengthened masonry structures will be discussed in Part II.

6. References

[1] Berto L, Saetta A, Scotta R, Vitaliani R (2002). An orthotropic damage model for masonry structures. Int J Numer Methods Engng 55: 127–57.

[2] Brasile, S., Casciaro, R., Formica, G. (2010). Finite Element formulation for non-linear analysis of masonry walls. Computers & Structures 88(3-4): 135-143

[3] Casolo, S. (1999). Rigid element model for non-linear analysis of masonry facades subjected to out-of-plane loading. Commun Numer Methods Eng 15(7): 457–468

[4] Casolo, S., Milani, G. (2010). A simplified homogenization-discrete element model for the non-linear static analysis of masonry walls out-of-plane loaded. Engineering Structures 32 (8): 2352-2366.

[5] CNR-DT 200 (2004). Guide for the design and construction of externally bonded FRP systems for strengthening existing structures. C.N.R. National Research Council, Italy.

[6] Cocchetti, G., Maier, G. (2003). Elastic-plastic and limit state analyses of frames with softening plastic-hinge models by mathematical programming. International Journal of Solids and Structures 40: 7219–7244.

[7] Colliat, J.B., Davenne, L., Ibrahimbegovic, A. (2002). Modélisation jusqu'à rupture de murs en maçonnerie chargés dans leur plan. Revue francaise de génie civil 4: 593-606.

[8] De Donato, O., Franchi, A. (1973). A modified gradient method for finite element elastoplastic analysis by quadratic programming. Computer Methods in Applied Mechanics and Engineering 2(2): 107-131.

[9] Denton, S.R., Morley, C.T. (2000). Limit analysis and strain softening structures. International Journal of Mechanical Sciences 42: 503-522.

[10] Di Pasquale, S. (1992). New trends in the analysis of masonry structures. Meccanica 27: 173-184.

[11] Fedele, R., Milani, G. (2010). A numerical insight into the response of masonry reinforced by FRP strips: the case of perfect adhesion. Composite Structures 92: 2345–2357.

[12] Gambarotta, L., Lagomarsino, S. (1997). Damage models for the seismic response of brick masonry shear walls. Part II: The continuum model and its applications. Earthquake Engineering and Structural Dynamics 26(4): 441-462.

[13] Grande, E., Milani, G., Sacco, E. (2008). Modelling and analysis of FRP-strengthened masonry panels. Engineering Structures, 30 (7), 1842-1860.

[14] Kaliszky, S. (1996). Elastoplastic analysis with limited plastic deformations and displacements. Mechanical Structures and Machines 24: 39–50.

[15] Kawai T (1978). New discrete models and their application to seismic response analysis of structures. Nuclear Engineering and Design 48: 207–229.

[16] Korany, Y., Drysdale, R., Chidiac, S.E. (2001). Retrofit of non-strengthened masonry buildings: The state-of-the-art. Proceedings of the 9th Canadian Masonry Symposium, Fredricton, New Brunswick, Canada, June 2001, 88–15.

[17] Koutromanos, I., Stavridis, A., Shing, P.B., Willam, K. (2011). Numerical modeling of masonry-infilled RC frames subjected to seismic loads. Computers & Structures 89(11-12): 1026-1037

[18] Lotfi, H.R., Shing, P.B. (1994). Interface model applied to fracture of masonry structures. Journal of Structural Engineering ASCE 120 (1): 63-80.

[19] Lourenço, P.B., de Borst, R., Rots, J.G. (1997). A plane stress softening plasticity model for orthotropic materials. International Journal for Numerical Methods in Engineering 40: 4033-4057.

[20] Lourenço, P.B., Mendes, N., Ramos, L.F., Oliveira, D.V. (2011). Analysis of masonry structures without box behavior, International Journal of Architectural Heritage, 5, 369-382.

[21] Lourenço, P.B., Milani, G., Tralli, A., Zucchini, A. (2007). Analysis of masonry structures: review of and recent trends of homogenisation techniques, Canadian Journal of Civil Engineering 34 (11): 1443-1457.

[22] Lourenço, P.B., Pina-Henriques, J.L. (2006). Masonry micro-modelling: a continuum approach in compression, Computers & Structures 84 (29-30): 1977-1989.

[23] Lourenço, P.B., Rots, J. (1997). A multi-surface interface model for the analysis of masonry structures. Journal of Engineering Mechanics ASCE 123 (7): 660-668.

[24] Luciano, R., Sacco, E. (1997). Homogenisation technique and damage model for old masonry material. International Journal of Solids and Structures 34 (24): 3191-3208.

[25] Luciano, R., Sacco, E. (1998). Damage of masonry panels reinforced by FRP sheets. Int J Solids Struct 35(15):1723–41.

[26] Mahini, S.S., Ronagh, H.R. and Eslami, A. (2007). Seismic rehabilitation of historical masonry vaults using FRPs. A case study. In Proc.: 1st Asia-Pacific Conference on FRP in Structures (APFIS 2007), S.T. Smith (Ed), University of Hong Kong and International Institute for FRP in Construction (IIFC), Hong Kong, China, 12-14 December 2007, 1: 565-570.

[27] Marfia, S., Sacco, E. (2001). Modelling of reinforced masonry elements. Int J Solids Struct 38:4177–98.

[28] Marques, R., Lourenço, P.B. (2011). Possibilities and comparison of structural component models for the seismic assessment of masonry buildings, Computers and Structures, 89(21-22), 2079-2091.

[29] Massart, T., Peerlings, R.H.J., Geers, M.G.D. (2004). Mesoscopic modeling of failure and damage-induced anisotropy in brick masonry. Eur J Mech A/Solids 23: 719–35.

[30] Milani, G., Lourenço, P.B., Tralli, A. (2006a). Homogenised limit analysis of masonry walls. Part I: failure surfaces. Computers and Structures 84: 166-180.

[31] Milani, G., Lourenço, P.B., Tralli, A. (2006b). Homogenization approach for the limit analysis of out-of-plane loaded masonry walls. Journal of Structural Engineering ASCE 132 (10): 1650-1663.

[32] Milani, G., Milani, E., Tralli, A. (2009). Upper Bound limit analysis model for FRP-reinforced masonry curved structures. Part II: structural analyses. Computers & Structures 87 (23-24): 1534–1558.

[33] Milani, G., Tralli, A. (2011). Simple SQP approach for out-of-plane loaded homogenized brickwork panels accounting for softening. Computers & Structures 89(1-2): 201–215.

[34] Milani, G., Tralli, A. (2012). A simple meso-macro model based on SQP for the non-linear analysis of masonry double curvature structures. International Journal of Solids and Structures, 49(5), 808-834.

[35] Milani, G. (2009). Homogenized limit analysis of FRP-reinforced masonry walls out-of-plane loaded. Computational Mechanics, 43, 617–639.

[36] Milani, G. (2011). Simple homogenization model for the non-linear analysis of in-plane loaded masonry walls. Computers & Structures, 89, 1586–1601.

[37] Pegon, P., Anthoine, A. (1997). Numerical strategies for solving continuum damage problems with softening: application to the homogenisation of masonry. Computers & Structures 64 (1-4): 623-642.

[38] Pietruszczak, S., Ushaksarei, R. (2002). Failure criterion for structural masonry based on critical plane approach Journal of Engineering Mechanics ASCE 128(7): 769-778.

[39] Pietruszczak, S., Ushaksarei, R. (2003). Description of inelastic behaviour of structural masonry. Int J Solids Struct 40: 4003–19.

7. Figures

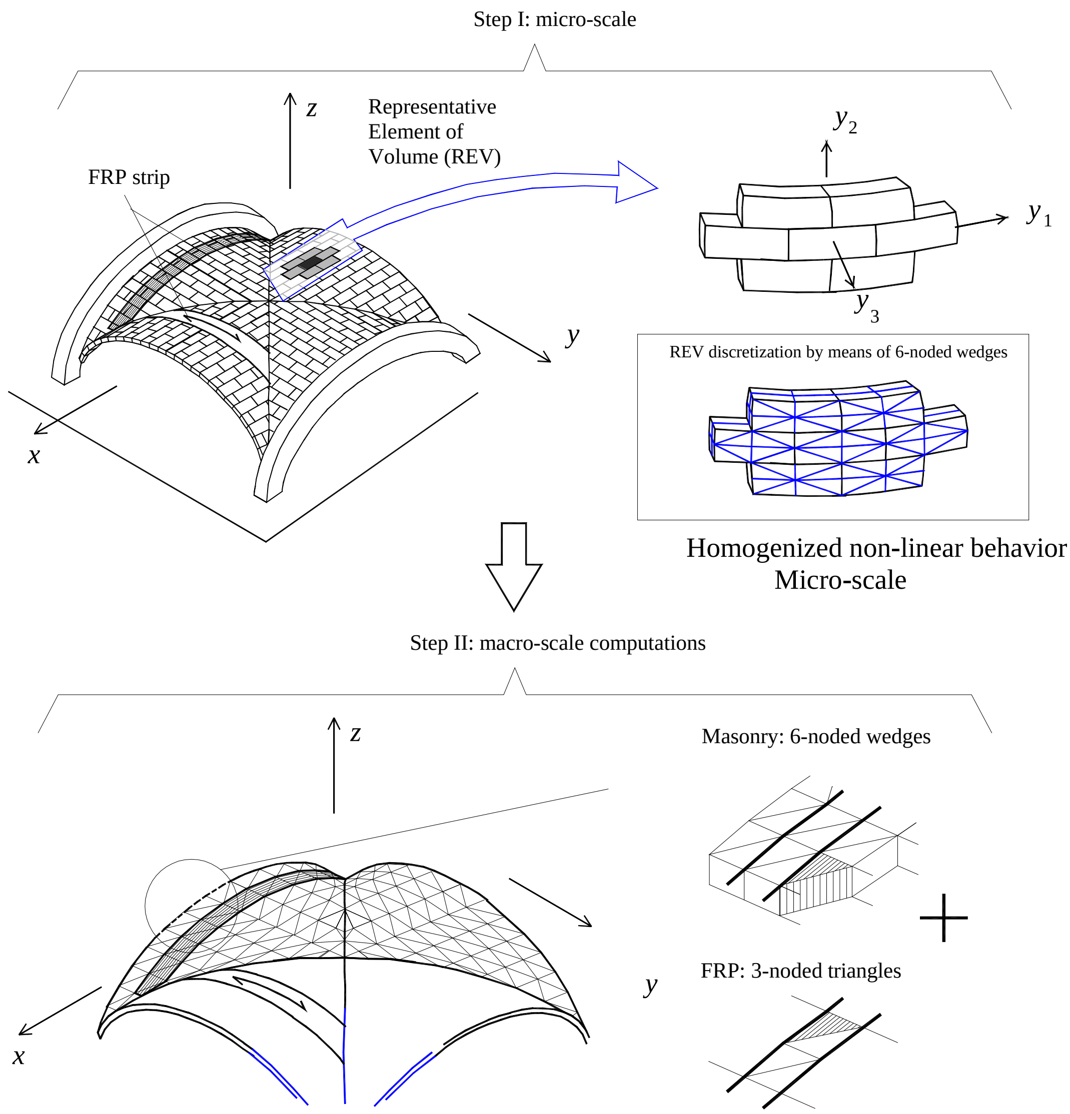

Figure 1: Two-step kinematic simplifying homogenization approach for the non-linear analysis of FRP reinforced masonry structures. Identification of a Representative Element of Volume (REV), subsequent evaluation of the non-linear non-strengthened macroscopic behavior of the REV, implementation at a structural level within a non-linear FE code (non-linear behavior of homogenized masonry and FRP).

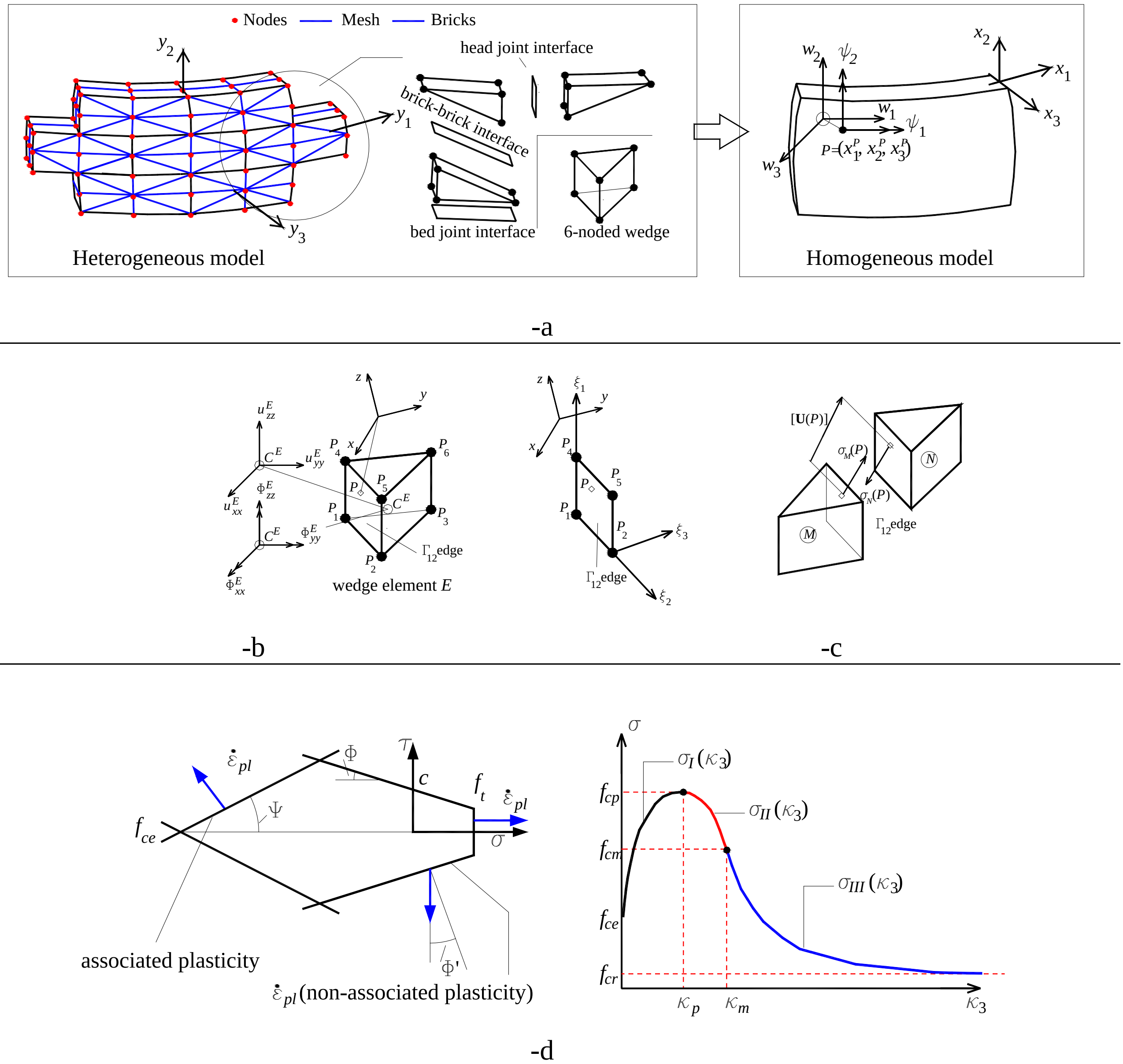

Figure 2: -a: FE discretization of the non-strengthened REV. –b: Rigid infinitely resistant six-noded wedge element used for the REV discretization.-c: Γ_{12} interface between contiguous elements. –d: Modified Mohr–Coulomb criterion for the mortar joint reduced to interface (left) and hardening/softening law in compression (right) as a function of the inelastic parameter κ_3

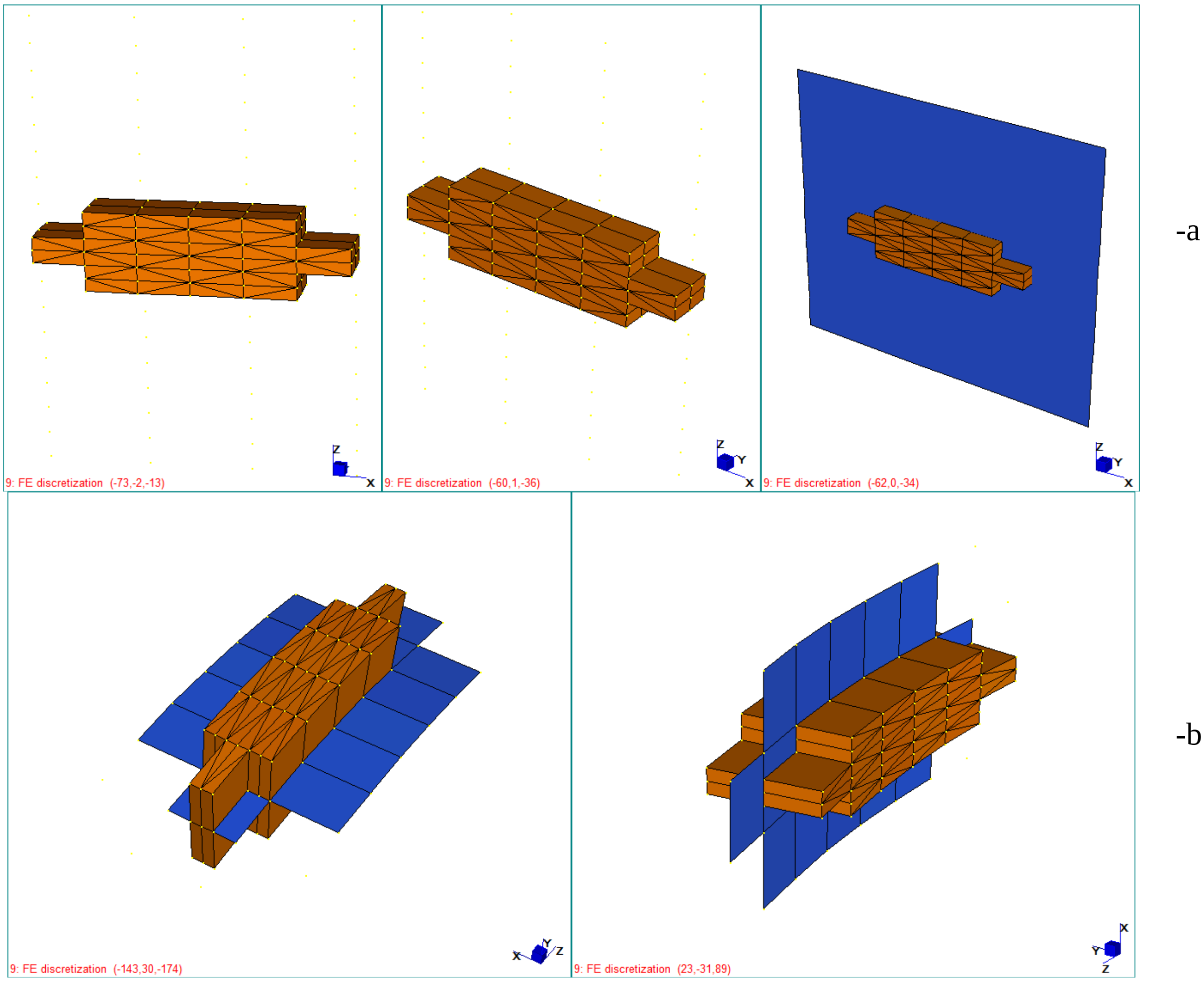

Figure 3: Masonry deep beam flat panel (-a) and circular arch (-b). Representative element of volume adopted for the simulations and FE discretization

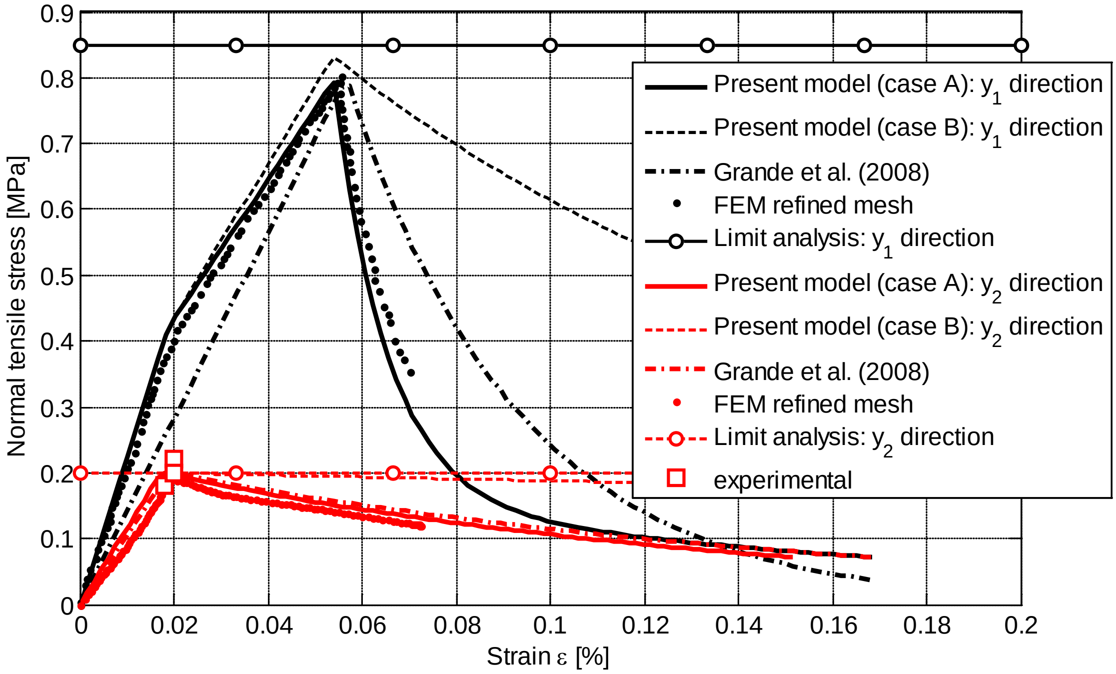

-a

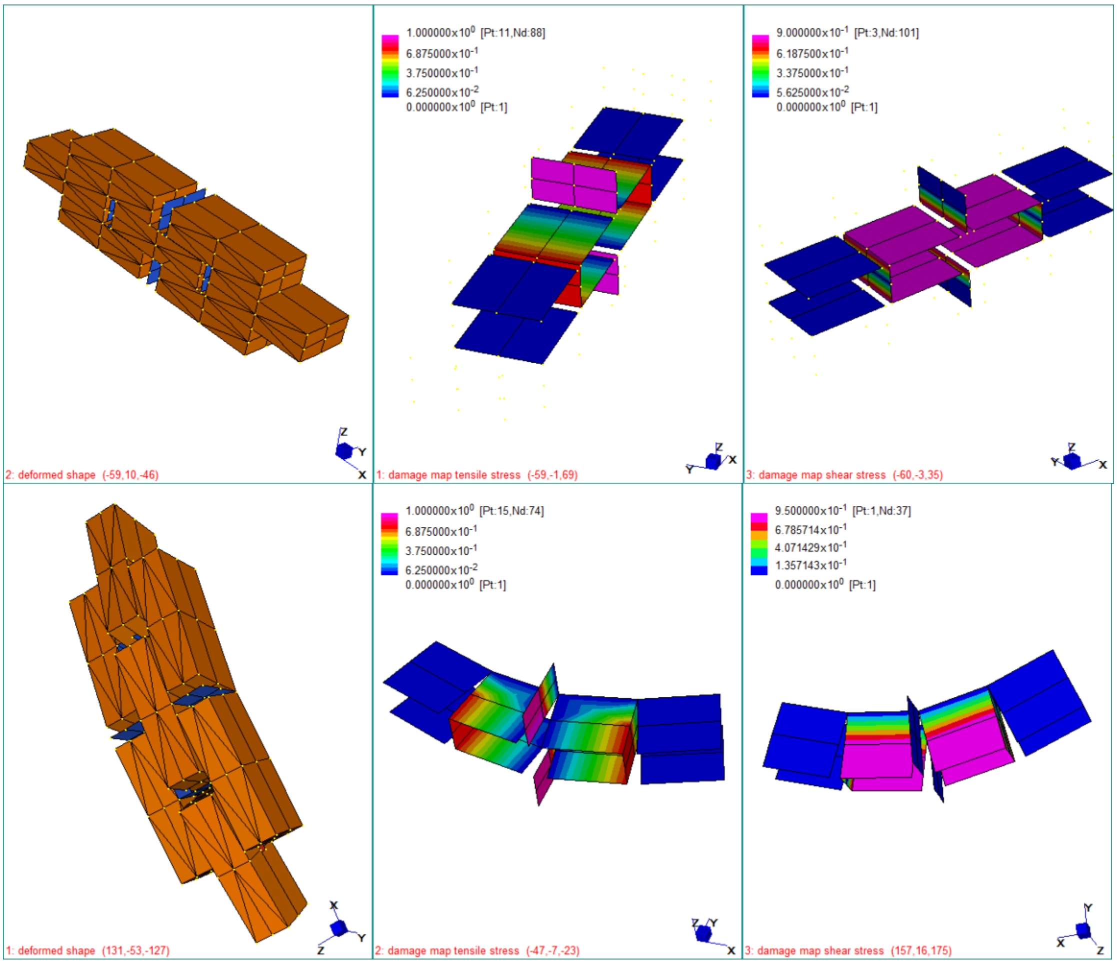

-b

Figure 4: Masonry deep beam -a: Uniaxial response of the homogenization model along horizontal and vertical tension for two values of fracture energy. -b: REV deformed shape at collapse for horizontal tension (mesh used and magnified view) with indication of interface damage in horizontal tension (center) and vertical tension (right). -c: same as previous, but for horizontal

bending.

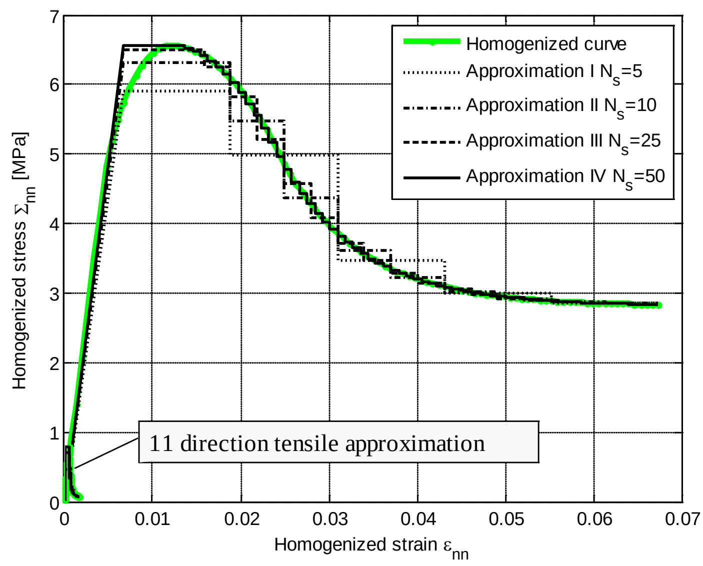

-a

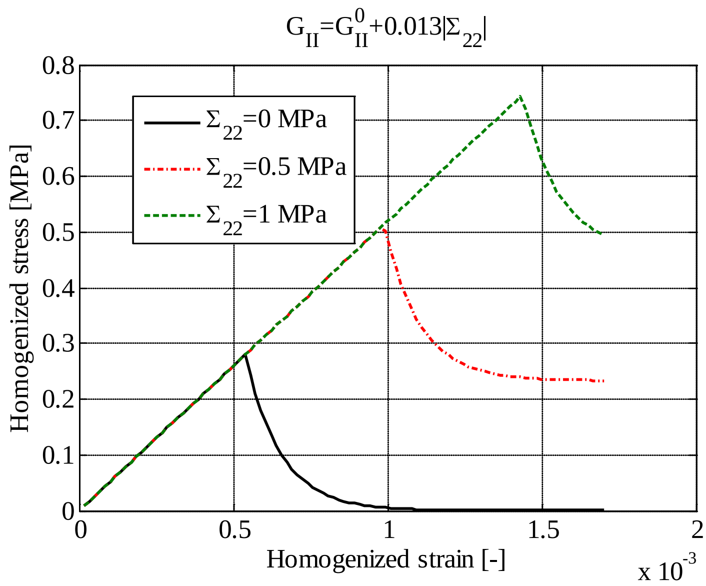

-b

-c

Figure 5: Masonry deep beam. Uniaxial response of the homogenization model. -a: vertical compression (with the linear piece-wise constant approximation used at a structural level). -b: shear behavior at three levels of increasing pre-compression.

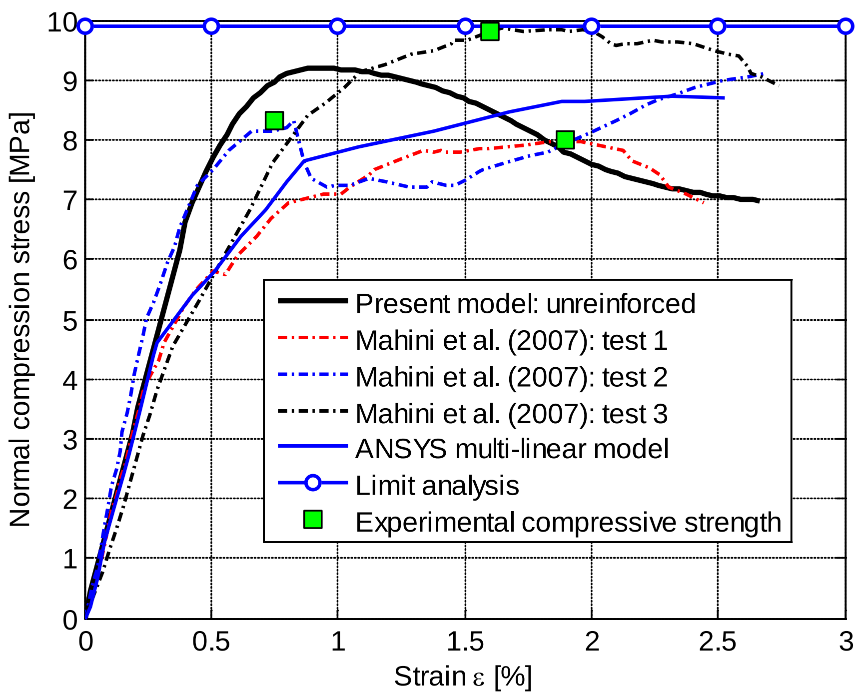

-a

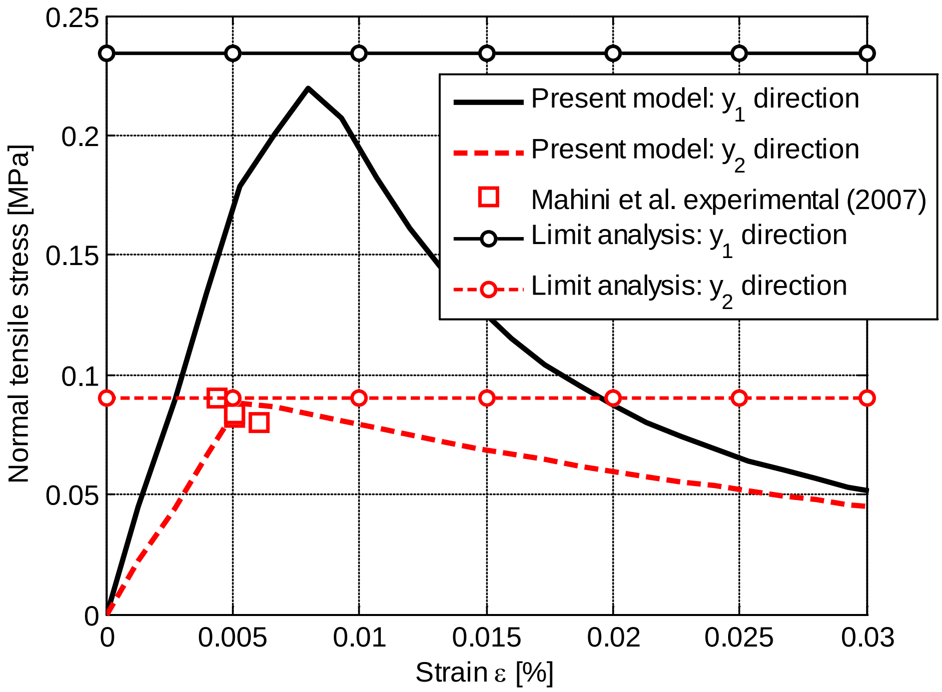

-b

Figure 6: Circular arch. a- REV compression behavior along parallels direction. –b: REV tensile membrane behavior.

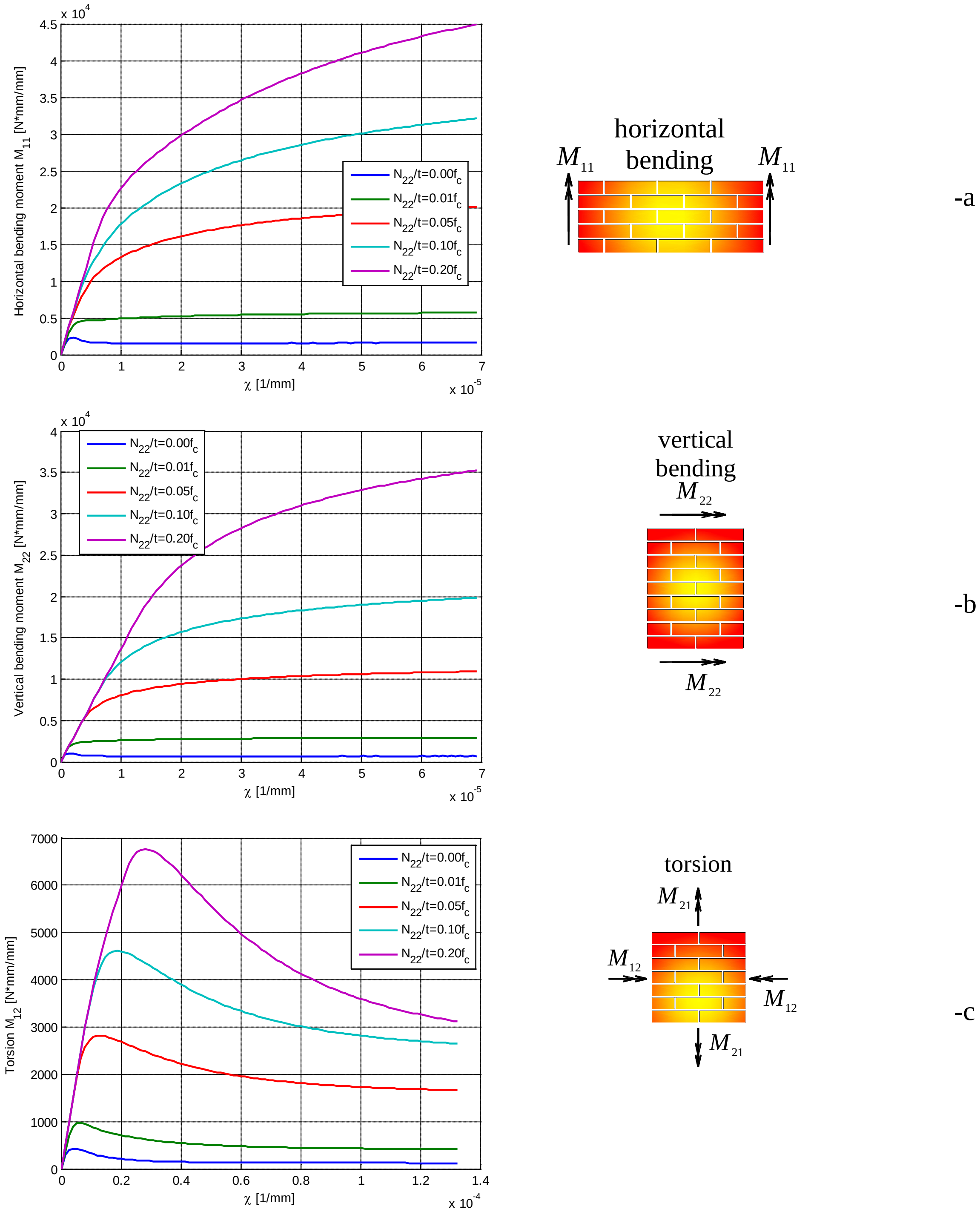

Figure 7: Circular arch. Flexural behavior of the REV, parabolic arch. Bending moment-curvature diagrams at increasing arch compressive load. -a: bending moment with hinge parallel to arch axis. -b: bending moment with hinge perpendicular to arch axis. -c: torsion.

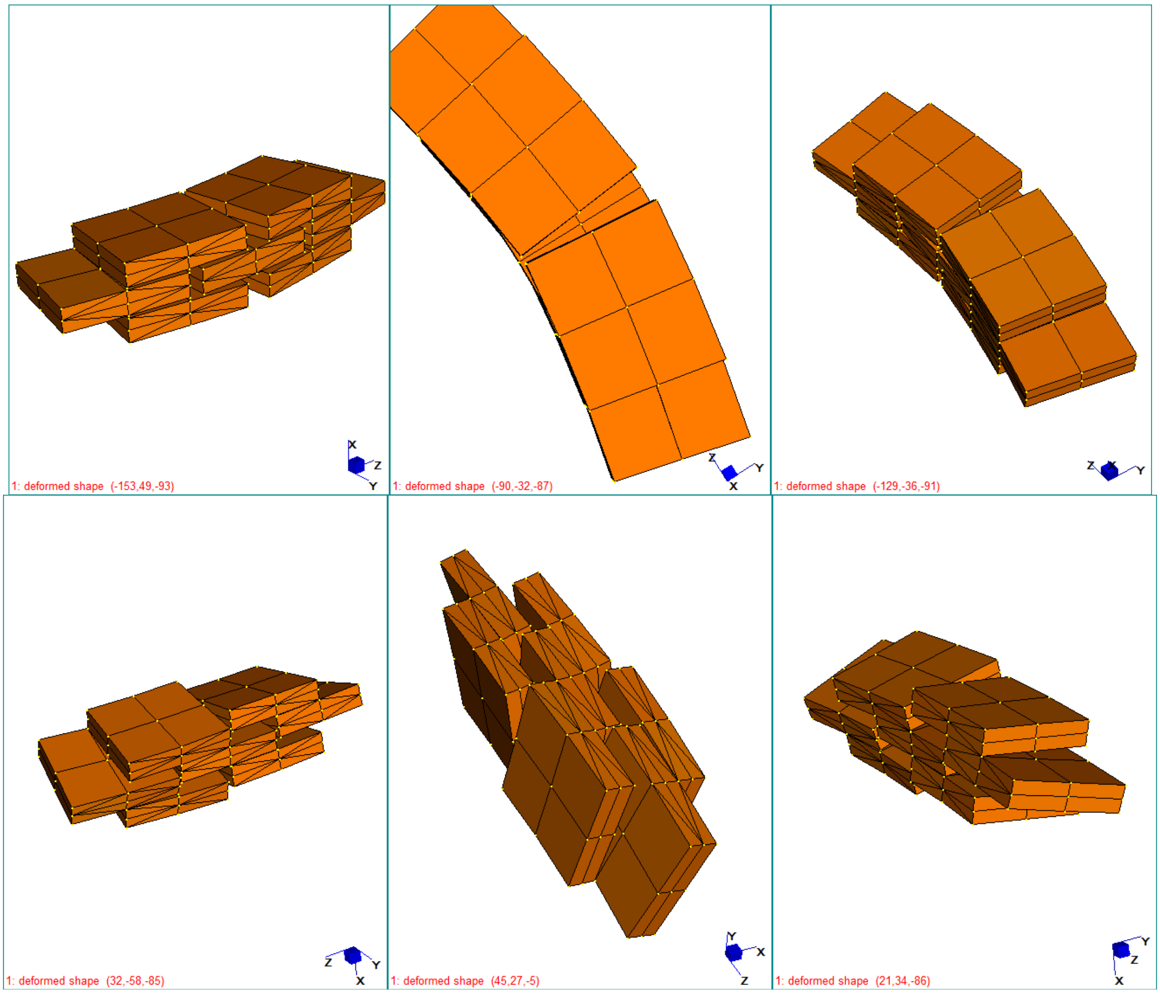

Figure 8: Circular arch. Typical REV deformed shapes at peak for (-a) pure M11 bending moment, (-b) pure M12 torsion

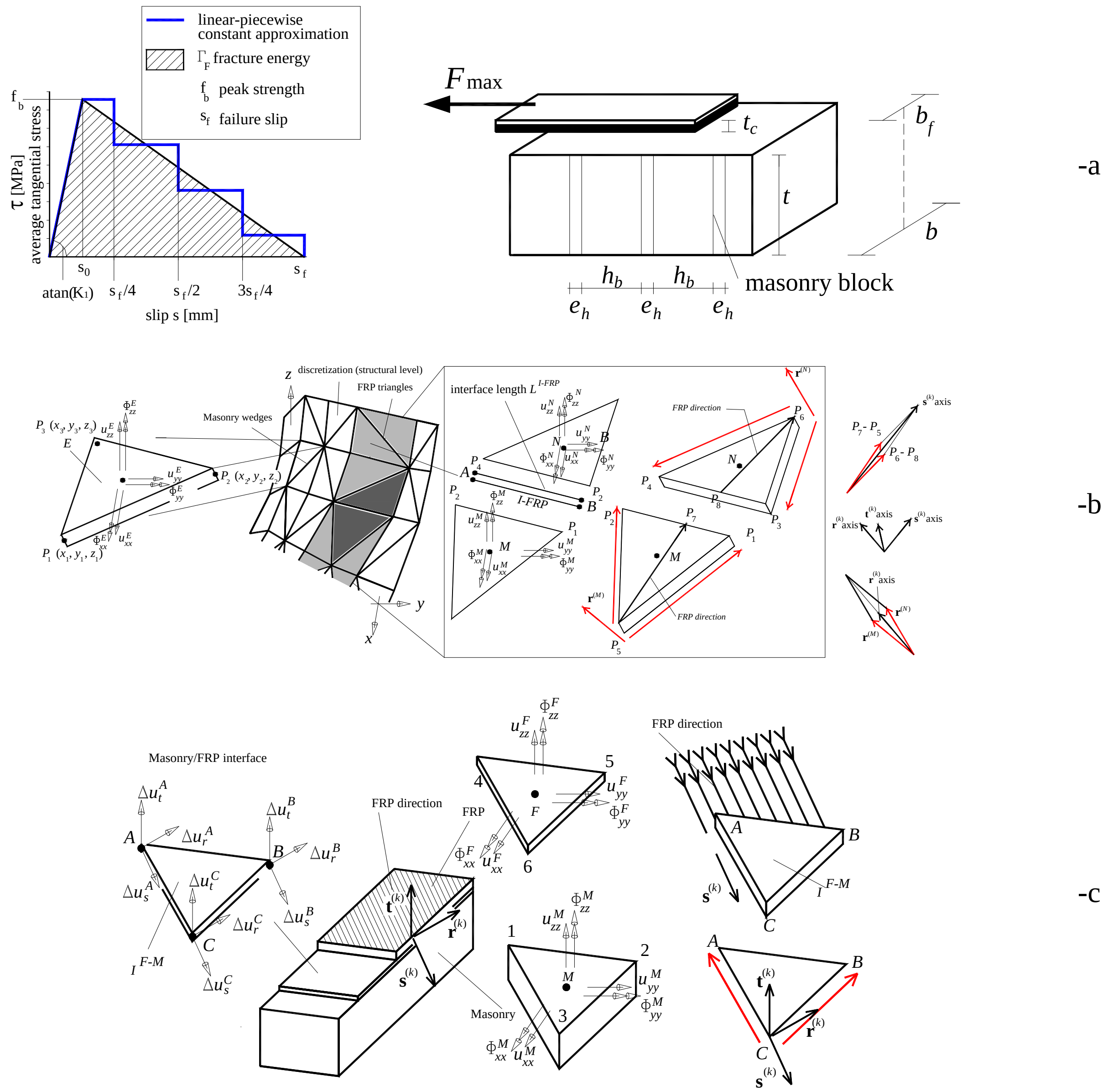

Figure 9: -a: FRP/masonry interface delamination law adopted (with its linear piecewise approximation). –b: FRP triangular element (left) and *A*-*B* interface between two contiguous *M*-*N* triangular FRP elements (right), with corresponding local frame of reference.-c: FRP/masonry interfaces. Discretization of interfaces with triangular elements interacting with FRP triangles and masonry wedges.

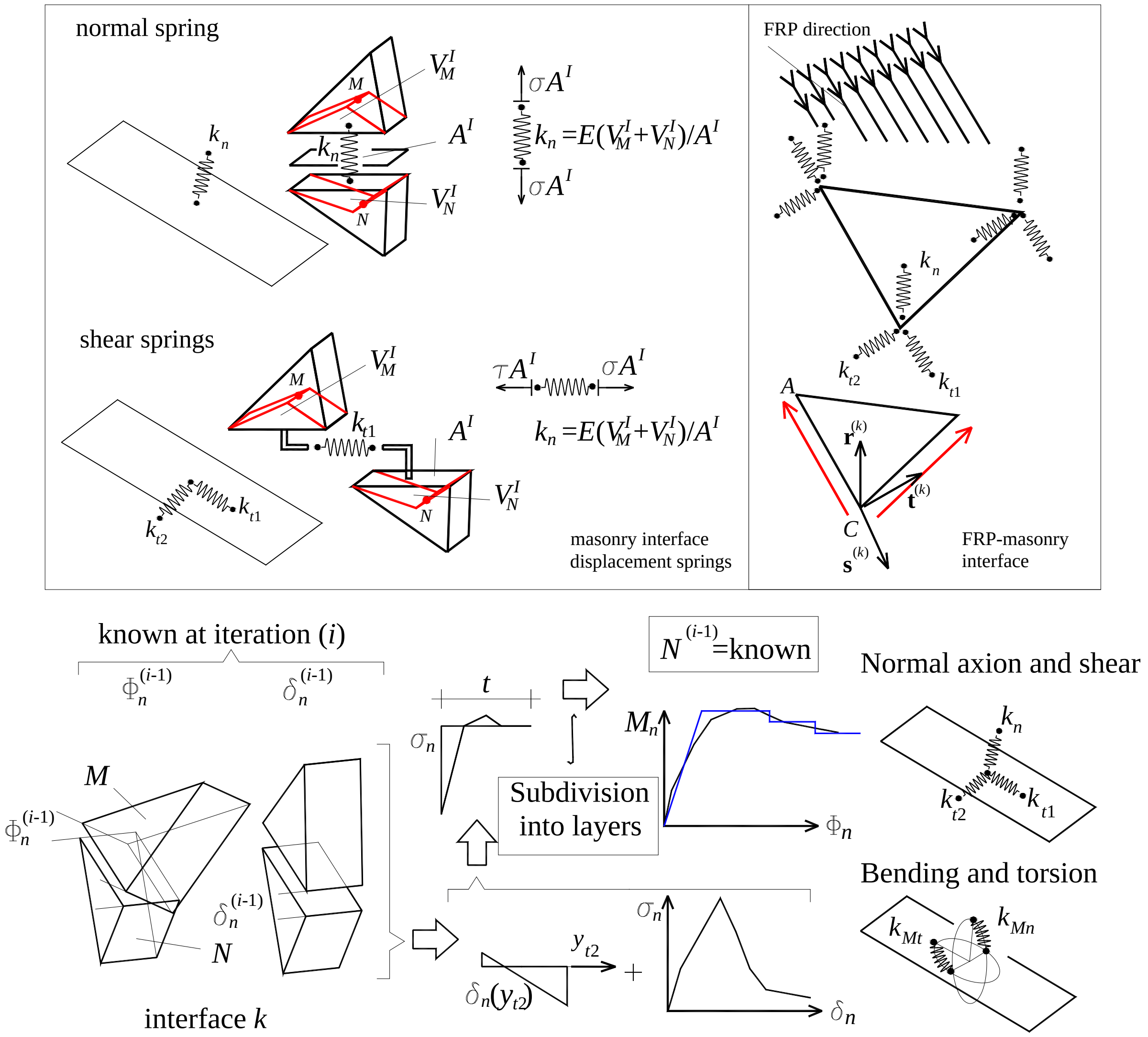

Figure 10: Top: schematic representation of displacement springs acting on masonry and FRP-masonry interfaces. Bottom: evaluation of the non linear load-displacement (or moment-rotation) behavior of the interfaces at each load step.

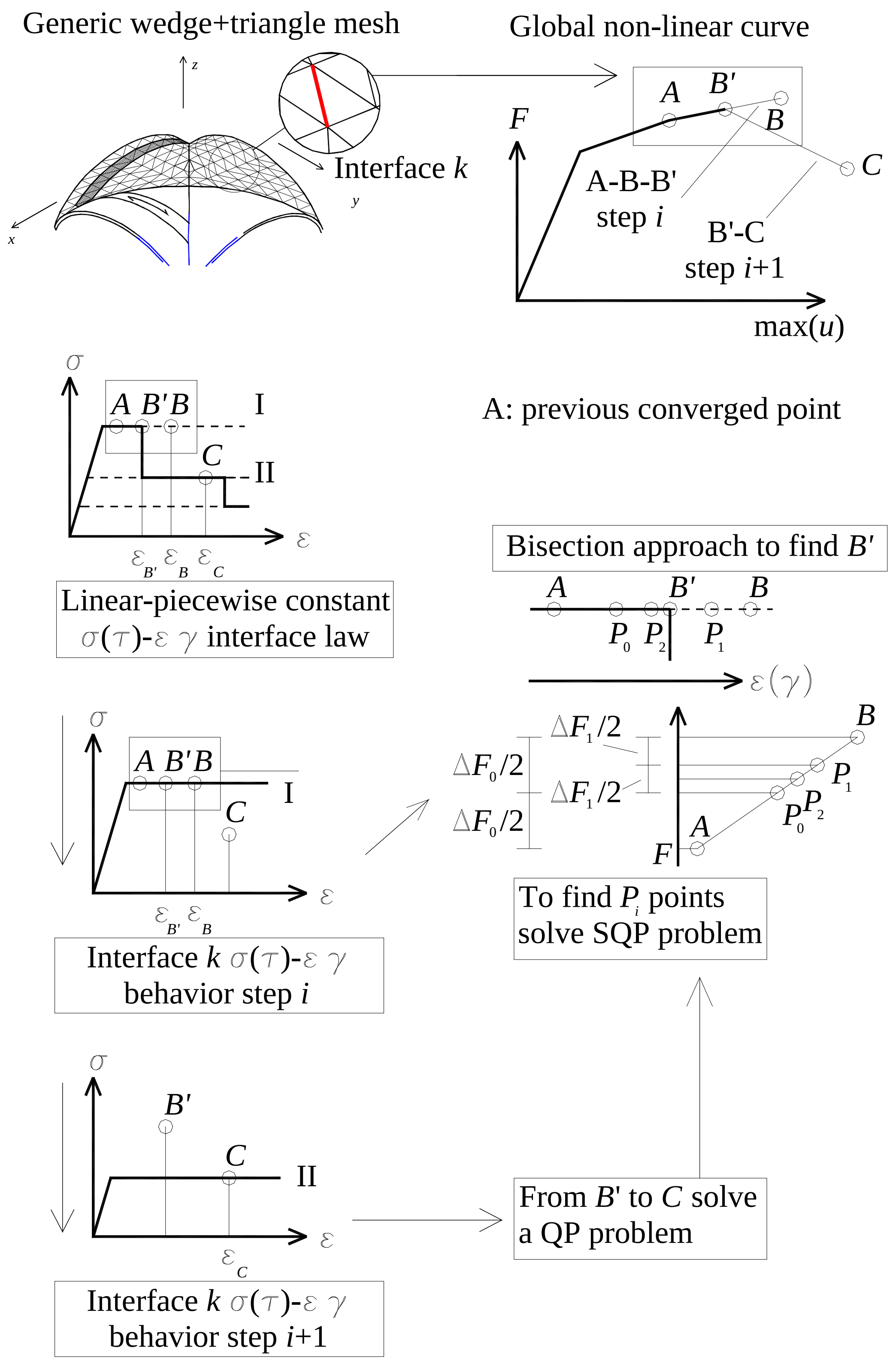

Figure 11: Sequential quadratic programming model used to handle deterioration of mechanical properties in the global non-linear response of the structure.

8. Tables

Table I: Masonry deep beam. Mechanical properties adopted for constituent materials.				
	joint	brick-brick interface		
E	700(*)	1600	[MPa]	Young Modulus
G	350(*)	800	[MPa]	Shear Modulus
c	1.4 f_t	2	[MPa]	Cohesion
f_t	0.2	-	[MPa]	Tensile strength
f_{ce}	$1/3 f_{cp}$	-	[MPa]	Compressive hardening/softening behavior
f_{cp}	7.5	-	[MPa]	
f_{cm}	$0.8 f_{cp}$	-	[MPa]	
f_{cr}	$0.5 f_{cp}$	-	[MPa]	
κ_p / e_h	$5\,\varepsilon_{el}$	-	[-]	
κ_m / e_h	$10\,\varepsilon_{el}$	-	[-]	
Φ	25	45	[°]	Friction angle
Ψ	45	-	[°]	Angle of the linearized compressive cap
G_f^I	0.02 (Case A) 0.2 (Case B)	10	[N/mm]	Mode I fracture energy
G_f^{II}	0.01 (Case A) 0.1 (Case B)	10	[N/mm]	Mode II fracture energy
(*) Interface stiffness is evaluated as E*(V1+V2)/(4A), with V1 and V2 being the volumes of the elements sharing the common interface under study and A being the interface area				

Table II: Circular arch. Mechanical properties adopted for constituent materials.				
	joint	brick-brick interface		
E	800$^{(*)}$	2200	[MPa]	Young Modulus
G	400$^{(*)}$	1000	[MPa]	Shear Modulus
c	0.8 f_t	2	[MPa]	Cohesion
f_t	0.09	-	[MPa]	Tensile strength
f_{ce}	1/4f_{cp}	-	[MPa]	Compressive hardening/softening behavior
f_{cp}	12	-	[MPa]	
f_{cm}	0.9f_{cp}	-	[MPa]	
f_{cr}	0.8f_{cp}	-	[MPa]	
κ_p / e_h	$5\,\varepsilon_{el}$	-	[-]	
κ_m / e_h	$10\,\varepsilon_{el}$	-	[-]	
Φ	27	45	[°]	Friction angle
Ψ	45	-	[°]	Angle of the linearized compressive cap
G_f^I	0.008	10	[N/mm]	Mode I fracture energy
G_f^{II}	0.005	10	[N/mm]	Mode II fracture energy
$^{(*)}$ Interface stiffness is evaluated as E*(V1+V2)/(4A), with V1 and V2 being the volumes of the elements sharing the common interface under study and A being the interface area				